

Remote Photonic Frequency-Upconversion using  
Semiconductor Optical Amplifiers for WDM /  
Broadband Radio-on-Fiber Applications

Young-Kwang Seo

The Graduate School

Yonsei University

Department of Electrical and Electronic Engineering

Remote Photonic Frequency-Upconversion using  
Semiconductor Optical Amplifiers for WDM /  
Broadband Radio-on-Fiber Applications

A Dissertation

Submitted to the Department of Electrical and Electronic Engineering

and the Graduate School of Yonsei University

in partial fulfillment of the

requirements for the degree of

Doctor of Philosophy

Young-Kwang Seo

January 2004

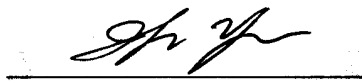
This certifies that the dissertation of Young-Kwang Seo is  
approved.



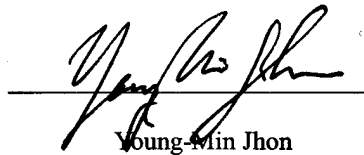
Thesis Supervisor: Woo-Young Choi



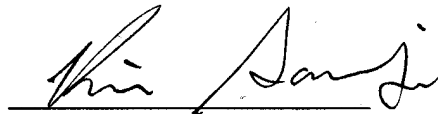
Sang-Yeol Lee



Ilgu Yun



Young-Win Jhon



Sangin Kim

The Graduate School

Yonsei University

January 2004

# Index

<b>Figure Index</b> .....	<b>iv</b>
<b>Abstract</b> .....	<b>vi</b>
<b>I. Introduction</b> .....	<b>1</b>
<b>II. Optical Heterodyne Local Oscillator Generation</b> .....	<b>14</b>
A. Single Sideband Modulation.....	16
B. Double Sideband-Suppressed Carrier Generation.....	19
C. Optical Phase-Locked Loop.....	22
D. Sideband Injection Locking .....	25
<b>III. Characteristics of Sideband Injection Locking</b> .....	<b>35</b>
<b>IV. SOA-based Photonic Frequency-Upconverter</b> .....	<b>48</b>
<b>V. WDM / Radio-on-Fiber Distribution</b> .....	<b>65</b>
<b>VI. Conclusions</b> .....	<b>74</b>
<b>Appendix</b> .....	<b>76</b>
<b>References</b> .....	<b>80</b>
<b>Abstract (in Korean)</b> .....	<b>85</b>

## Figure Index

Figure 1.1 Hybrid integration of wireless and fiber-optic communications .....	3
Figure 1.2 Typical radio-on-fiber configurations. (a) Optical radio frequency transmission and (b) IF feeder.....	5
Figure 1.3 Fiber dispersion-induced signal suppression for $f_{LO}$ of 30 GHz in Fig. 1.2(a) .....	6
Figure 1.4 Photonic frequency-upconverter using a semiconductor optical amplifier .....	9
Figure 1.5 Proposed radio-on-fiber configuration .....	10
Figure 2.1 Optical single-sideband modulation using a dual-electrode Mach-Zehnder intensity modulators .....	17
Figure 2.2 Double sideband-suppressed carrier modulation using Mach-Zehnder intensity modulators.....	21
Figure 2.3 Block diagram for optical phase-locked loop .....	24
Figure 2.4 Block diagram for the optical micro-/ millimeter-wave generation with sideband injection locking .....	26
Figure 2.5 Optical spectra of the RF-modulated ML (thin) and two slave lasers (bold) injection-locked to $\pm 3$ ML sidebands .....	29
Figure 2.6 RF-spectrum (a) and single sideband phase-noise (b) of the 60-GHz beat signals between two injection-locked slave lasers in Fig. 2.4. ....	30
Figure 2.7 Long-term intensity variations (a) and single-sideband phase-noises at 100 kHz offset frequency (b) of the LO source generated with sideband injection locking.....	31

Figure 3.1 Calculated stable-locking range for $\pm 2$ target sidebands .....	39
Figure 3.2 Calculated optical and RF-spectra of sideband injection-locked SLs for the different $R$ 's .....	40
Figure 3.3 Dependence of $\Delta P$ and stable-locking bandwidth .....	43
Figure 3.4 Experimental setup for sideband injection locking .....	44
Figure 3.5 Measured (a) RF-spectrum for estimated $R = -16$ dB and, (b) $\Delta P$ and stable-locking bandwidth for different $R$ 's .....	46
Figure 4.1 Experimental setup for photonic frequency-upconverter .....	49
Figure 4.2 Calculated (a) and experimental (b) results of signal frequency- upconversion efficiency with LO light intensity .....	56
Figure 4.3 Frequency-upconversion efficiency for different SOA input wavelengths .....	57
Figure 4.4 Calculated frequency responses of the frequency-upconversion efficiency for different SOA bias currents .....	60
Figure 4.5 Normalized SOA cross-gain modulation (XGM) response .....	61
Figure 4.6 Measured LO frequency responses .....	64
Figure 5.1 WDM / 60-GHz radio-on-fiber distribution configuration .....	53
Figure 5.2 Measured optical spectra for (a) base station #1 and (b) base station #2 after AWG .....	67
Figure 5.3 Measured RF-spectrum of frequency-upconverted 622 Mbps data with the 60-GHz optical LO signal for base station #2 .....	71
Figure 5.4 Bit error rate (a) and eye-diagram (b) of recovered 622 Mbps data after 20-km fiber-optic link in Fig. 5.1 .....	72
Figure 5.5 Measured eye-diagrams of recovered 622 Mbps data for (a) base station #1 and (b) base station #2 .....	73

## **Abstract**

### **Photonic Frequency-Upconversion using Semiconductor Optical Amplifiers for WDM / Radio-on-Fiber Applications**

Seo, Young-Kwang

Dept. of Electrical and Electronic Eng.

The Graduate School

Yonsei University

A novel photonic frequency-upconversion has been proposed where the frequency-upconversion of optical base-band or intermediate frequency (IF)-band signals with optical local oscillator (LO) source is achieved with the cross-gain modulation of a semiconductor optical amplifier (SOA) and the square-law photo-detection of a photo-diode. For avoiding fiber dispersion effects, the optical LO source is produced by the sideband injection locking as optical heterodyne method to have two optical modes separated by the desired LO frequency in the optical spectrum. The detected LO signal as beat signals between two optical modes has a narrow linewidth and long-term intensity stability.

From the numerical analysis of the proposed photonic frequency-

upconverter based on the linearized SOA rate-equations, it is found that the conversion is directly attributed by the SOA optical gain and can be optimized by either controlling the optical powers of optical LO power or selecting the optical IF and LO wavelengths. The experimental verification was qualitatively performed as well.

Using these useful features, a 60-GHz radio-on-fiber distribution scheme of 2 x 622Mbps digital WDM channels is experimentally demonstrated, where two WDM channel are frequency-upconverted with a single 60-GHz optical LO source remotely at base stations after 20-km fiber-optic link and are re-transmitted over 3-meter wireless link. This proposed scheme would be useful in radio-on-fiber systems where one optical LO signal is shared among multiple base stations addressed by their wavelengths.

---

Keywords: radio-on-fiber, semiconductor optical amplifier, cross-gain modulation, sideband injection locking, optical heterodyne method, remote photonic frequency-upconversion, conversion efficiency, wavelength-division multiplexing



## **I. Introduction**

There has been the great progression in information and communication networks up to recently. The move to the mobile and broadband local access in the wireless and wired communications is outstanding and will ultimately allow broadband communication anything, anytime and anywhere. In particular, the wireless communication has seen the tremendous increase in the number of mobile phone subscribers and expanded their services from voice and short messages to video streaming and wireless internet. In order to allow more subscribers and better services, it is expected to utilize millimeter-wave bands in a next-generation wireless system that will provide more radio spectrum resource and better frequency reuse due to reduced cell size.

The fixed lines for the wired communication should be implemented using optical fiber to increase data rate. The fiber-optic systems now play a key role in the long-haul communication traffic and can have a channel rate of 10 Gbps commercially. With the progressive evolution of Ethernet standard, the optical fiber is penetrating itself into broadband local access. Although the wired communication is suitable for the higher data rate services, it does not allow communications

anywhere. Therefore, the wired and wireless communication technologies will be likely integrated together in the next-generation communications. Their interdisciplinary research area has been introduced as radio-on-fiber or microwave photonics [1]. The definition of “radio” here represents electromagnetic waves in radio frequency (RF) and even in microwave and millimeter-wave band.

In the typical digital fiber-optic communications, the baseband digital bit stream, combinations of symbol ‘ones’ and ‘zeros’, is delivered over optical fiber. In the radio-on-fiber system, however, the various kinds of services, such as PSTN, ATM and internet, are collected in one central office and re-distributed through fiber-optic links to multiple base-stations without demodulation before the fiber-optic link and re-modulation before the antenna link. In each base-station, the information arrived from the central office should be eventually re-transmitted in free space to end-users over the wireless antenna link, as described in Fig. 1.1. The radio-on-fiber can find applications in broadband radio access, such as indoor wireless LAN [2], mobile communication [3], intelligent transportation system [4], military warfare [5] and radio astronomy [6].

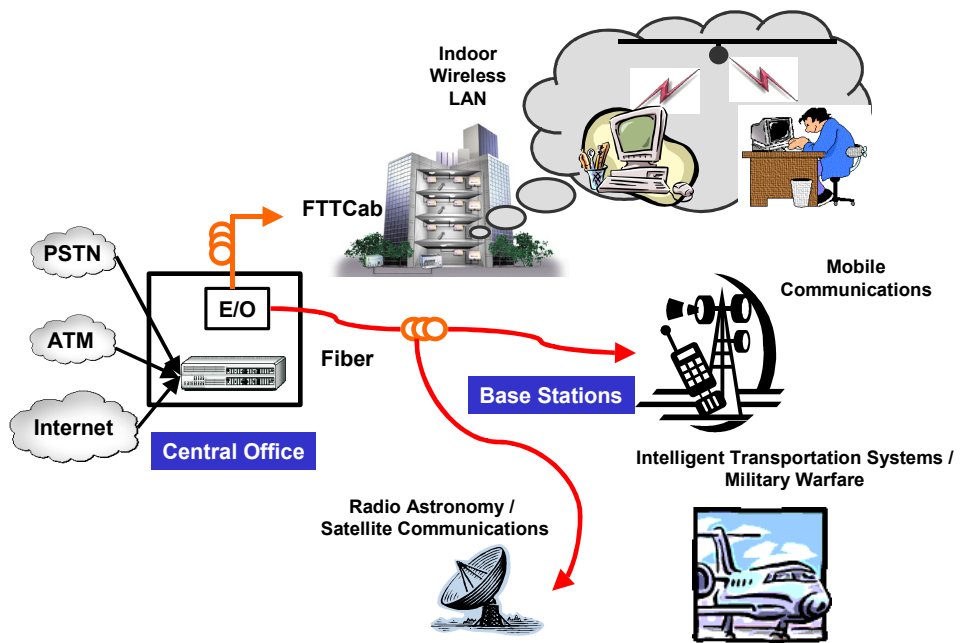
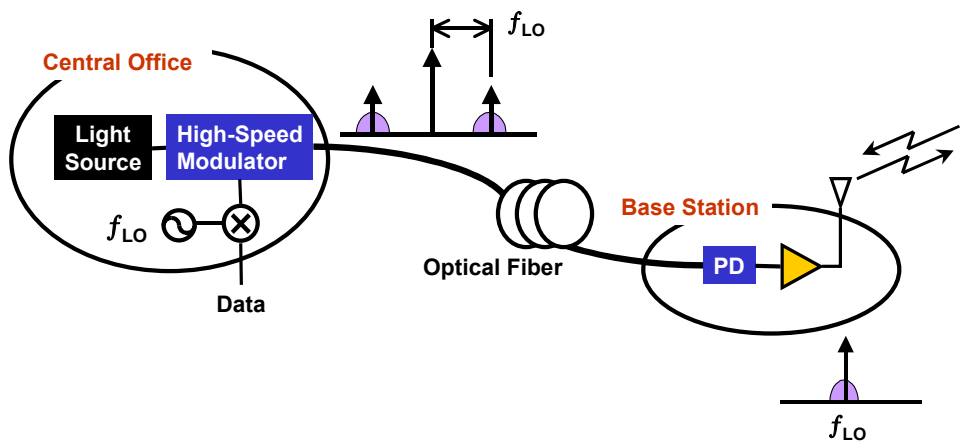


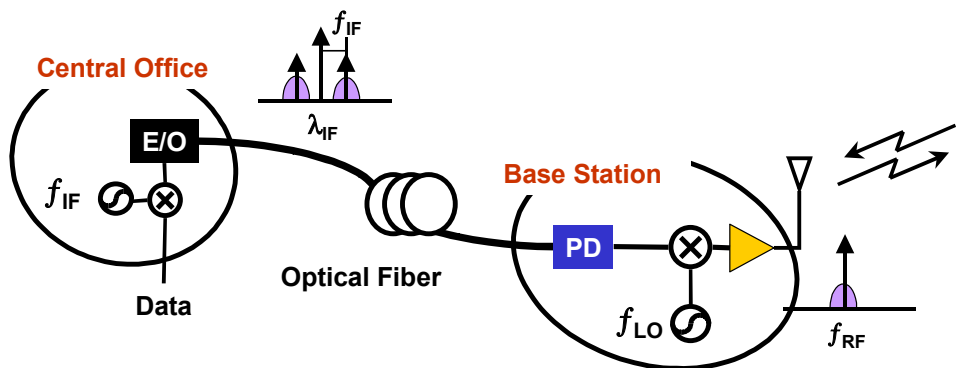
Fig. 1.1. Hybrid integration of wireless and fiber-optic communications

The broadband radio access requires a large number of base stations due to the small cell size. The base-stations should be compact and simple in implementation. A simple approach to transmit radio signals over fiber-optic links is to employ high-speed intensity modulators as illustrated in Fig. 1.2(a). The optical carrier is intensity-modulated with high-speed optical modulators in a central office. The modulated signals are transmitted to and photo-detected in base-stations. It is called as “intensity-modulation and direct-detection” [7]. This approach can make base stations simple because the photo-detected RF-signals in base stations are just electrically amplified and re-transmitted over the wireless antenna link. The complex and expensive equipment, such as high-speed optical modulator, electrical local oscillator (LO) and mixer operating at the very high radio frequencies, can be centralized in one central office and their costs can be also shared among multiple base stations.

This approach is, however, sensitive to fiber chromatic dispersion effect, which will degrade system performance. The intensity-modulation of the optical light produces two sidebands separated by the modulation frequency  $f_{LO}$  from the optical carrier  $\lambda_C$  in the optical spectral domain. As they propagate through dispersive optical fibers, two sidebands experience different phase-shifts because they travel in



(a)



(b)

Fig. 1.2. Typical radio-on-fiber configurations. (a) Optical radio frequency transmission and (b) IF feeder.

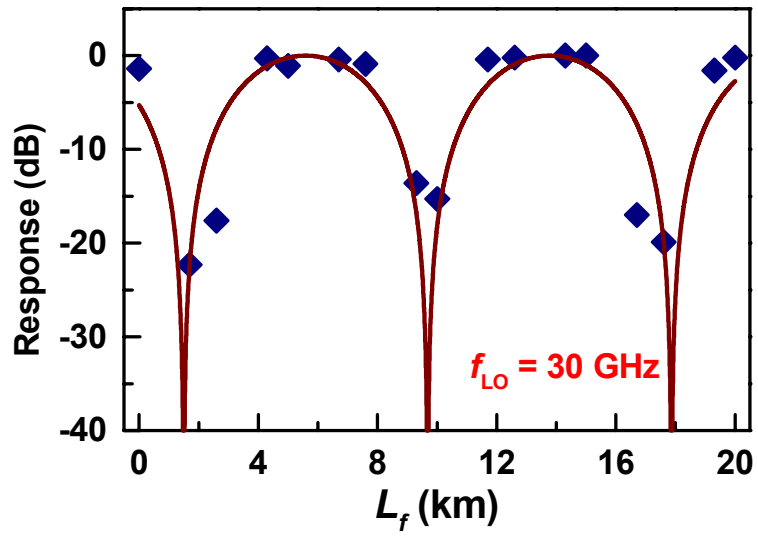


Fig. 1.3. Fiber dispersion-induced signal suppression for  $f_{LO}$  of 30 GHz in Fig. 1.2 (a).

different velocities owing to fiber chromatic dispersion. Whenever the relative phase difference between two sidebands becomes out of phase, the photo-detected signal powers at  $f_{LO}$  are greatly and periodically suppressed. Its relationship can be represented by [8]

$$P_{LO} \propto \cos^2 \left[ \frac{\pi \lambda_c^2 D L_f f_{LO}^2}{c} + \arctan(\alpha) \right] \quad (1.1)$$

where  $D$  represents the fiber dispersion,  $L_f$  the fiber length,  $\lambda_c$  the center optical carrier wavelength,  $f_{LO}$  the electrical modulation frequency,  $P_{LO}$  the photo-detected signal power at  $f_{LO}$  and  $\alpha$  the modulator chirp. The derivation of Eq. (1.1) is given in Appendix.

In order to investigate the effect of fiber chromatic dispersion, photo-detected signal powers were measured as function of fiber transmission length when the high-speed optical modulator was intensity-modulated at  $f_{LO}$  of 30 GHz. The results are shown in Fig. 1.3. For the compensation of the optical loss in fiber transmission, an Erbium-doped fiber amplifier and a variable optical attenuator were employed before photo-detection. The solid line in the figure is obtained from curve-fitting the modulated signal power measurement results with Eq. (1.1). Fig. 1.3 shows that the photo-detected LO power

$P_{LO}$  is periodically suppressed at  $L_f = \frac{c}{2\lambda_c^2 D f_{LO}^2} \left( 1 + 2k - \frac{2}{\pi} \arctan(\alpha) \right)$  (for  $k = 0, 1, 2, \dots$ ) as can be predicted in Eq. (1.1). In order to avoid dispersion-induced penalties, various optical heterodyne schemes for use in fiber-optic delivery of RF-signals have been demonstrated and their features will be discussed in Section II.

One alternative approach is to send base-band or intermediate frequency (IF) signals through optical fiber. Then, the photo-detected signals at each base-station should be frequency-upconverted to the desired radio frequency as illustrated in Fig. 1.2(b). The IF frequency used for signal processing in the central station is relatively much lower than the radio frequency for the wireless link in base-stations. One can find from Eq. (1.1) that the dispersion-induced signal suppression effects become much less severe with the employment of the lower modulation frequency used in the central station before fiber-optic link. Since the IF frequencies are typically less than several gigahertz in practice, this approach is relatively insensitive to fiber chromatic dispersion effects. But, it will make the base-stations more complex and expensive in design and implementation because every base-station needs high-frequency electrical mixers and LO sources for the photo-detected IF-signals to be frequency-upconverted and re-transmitted over wireless antenna links.



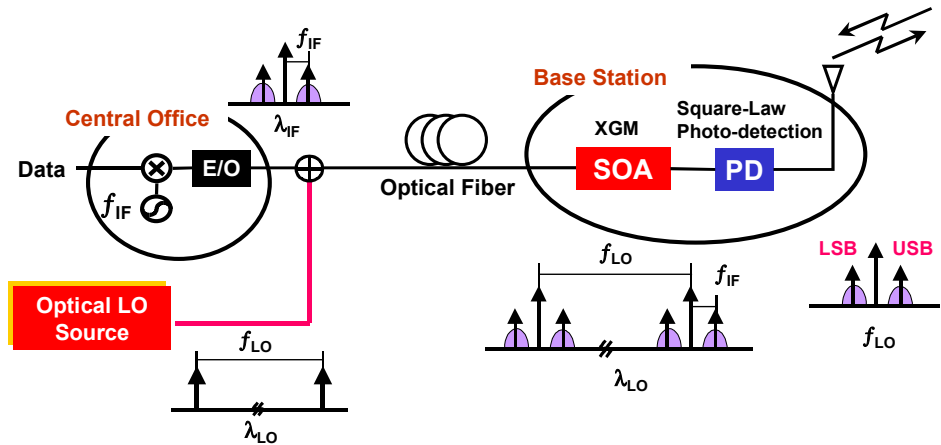


Fig. 1.4. Photonic frequency-upconverter using a semiconductor optical amplifier

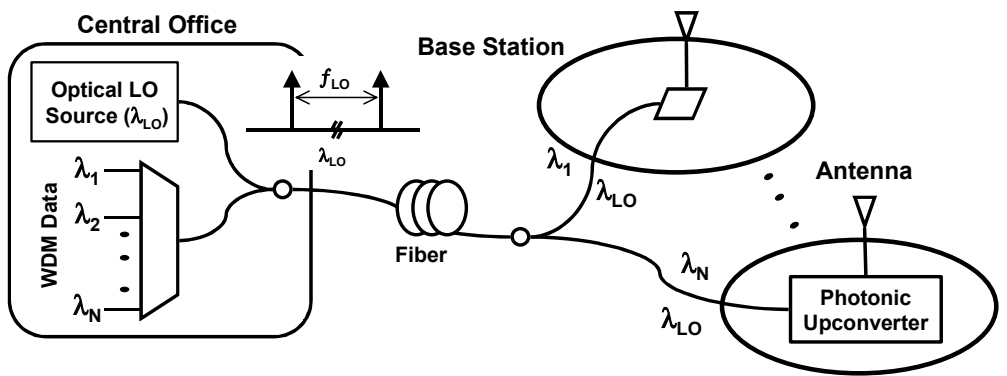


Fig. 1.5. Proposed radio-on-fiber configuration.

This dissertation proposes a novel photonic frequency-upconverter using a semiconductor optical amplifier as shown in Fig. 1.4, where the optical LO signal is transmitted along with the optical IF signal having different wavelengths in a central station [9-12]. To neglect the fiber dispersion effect in transmission, the optical IF signal carries data in baseband or IF-band as like the case in Fig. 1.3, and the optical LO signal under consideration has two optical modes separated by the desired LO frequency. For this, optical heterodyne methods are employed for the generation of optical LO sources. At a base station, the data carried in the optical IF signal is frequency-upconverted with the optical LO signal by using a photonic frequency-upconverter. In [13], a photonic frequency-upconverter was constructed by taking advantage of the nonlinear photo-detection behavior of a high-speed photo-detector (PD). This signal upconversion scheme, however, has low conversion efficiency.

In this dissertation, a semiconductor optical amplifier (SOA) is employed for the better conversion efficiency. All optical frequency-upconversion of the IF-band signal ( $f_{IF}$ ) to lower sideband (LSB,  $f_{LO} - f_{IF}$ ) and upper sideband (USB,  $f_{LO} + f_{IF}$ ) with an optical LO source is achieved in combination with the SOA cross-gain modulation and square-law photo-detection of a photo-diode (PD) as described in Fig.

1.4. The mixing of two RF-modulated optical signals in SOA has been demonstrated in [14]. In this case, however, the RF modulation of both optical signals was limited within the SOA gain modulation bandwidth that is typically less than 10 GHz. In this dissertation, it is demonstrated that such limitation is not necessary for both optical LO and IF signals. If only one of them (in this case, IF-frequency) is within the SOA gain modulation bandwidth, successful upconversion is possible. It should be noted that this IF frequency limit for the optical IF signal will not pose any problem in applications, because the typical radio-on-fiber systems have IF frequencies not exceeding the gigahertz range. In addition, our scheme does not have wavelength- or polarization-dependence, and signal upconversion is possible for a wide range of separation between IF and LO wavelengths as long as both are within the range of SOA optical gain.

Using this proposed SOA-based photonic frequency-upconverter, this dissertation demonstrates a new radio-on-fiber distribution scheme as illustrated in Fig. 1.5 [9, 12], where wavelength division multiplexing (WDM) technique is employed in the radio-on-fiber systems to increase the total data traffic capacity. One optical LO signal is distributed to several base stations and multiple base-band or IF-band WDM data are wavelength-selectively transmitted to base stations. One

optical LO source is distributed to and shared among base-stations. The WDM data and optical LO source have different wavelengths in the optical spectrum. The WDM data are remotely frequency-upconverted with the optical LO source by utilizing the proposed SOA-based photonic upconverter at each base-station.

This dissertation is organized as follows. Section II deals with optical heterodyne methods for the generation of the optical LO sources that should have two optical modes separated by the desired LO frequency. In particular, the characteristics of the sideband injection locking method are discussed numerically and experimentally in more details in Section III. Section IV deals with the proposed photonic upconverter based on the SOA cross-gain modulation and the PD square-law photo-detection behavior. In this section, the operation principle and characteristics as well as numerical and experimental analyses are given. Section V deals with the a new WDM / fiber-radio access distribution architecture where broadband digital WDM data are frequency-upconverted with the SOA-based photonic upconverter remotely at base-stations after fiber-optic link and re-transmitted over 60-GHz antenna link And, conclusions are given in Section VI.

## II. Optical Heterodyne Local Oscillator Generation

In order to avoid the fiber dispersion-induced penalty problem, optical heterodyne methods under consideration should be taken for the optical LO source to have two optical modes separated by the desired LO frequency. When these optical modes are photo-detected, they beat each other owing to the PD square-law photo-detection feature and produce their beat signal at the frequency that is same as their optical frequency difference. To model this situation, an optical heterodyne LO source can be assumed to have two independent optical modes with optical angular frequency of  $\omega_1$  and  $\omega_2$  [15]:

$$\begin{aligned} E_1(t) &= \sqrt{P_1} e^{j[\omega_1 t + \Phi_1(t)]} \quad \text{and} \\ E_2(t) &= \sqrt{P_2} e^{j[\omega_2 t + \Phi_2(t)]}. \end{aligned} \quad (2.1)$$

where  $P_i$  is the average optical power and  $\Phi_i$  the optical phase for  $i = 1$  and 2. When these two optical modes,  $E_1$  and  $E_2$ , propagate through the dispersive fiber with the slightly different velocities, they will experience the relative phase difference  $\theta_D$ . The electric fields after the fiber can be written by:

$$\begin{aligned}\widehat{E}_1(t) &= \sqrt{P_1} e^{j[\omega_1 t + \Phi_1(t)]} \quad \text{and} \\ \widehat{E}_2(t) &= \sqrt{P_2} e^{j[\omega_2 t + \Phi_2(t) + \theta_D]}.\end{aligned}\tag{2.2}$$

the photo-detected current  $I_{PD}$  in PD is given by

$$\begin{aligned}I_{PD} &= R_{PD} (\widehat{E}_1 + \widehat{E}_2)^* \cdot (\widehat{E}_1 + \widehat{E}_2) \\ &= R_{PD} \left\{ P_1 + P_2 + 2\sqrt{P_1 \cdot P_2} \cos \left[ |\omega_2 - \omega_1| t + |\Phi_2 - \Phi_1| + \theta_D \right] \right\},\end{aligned}\tag{2.3}$$

where  $R_{PD}$  represents PD responsivity. Eq. (2.3) shows that the electrical beat signal at the optical frequency difference  $|\omega_2 - \omega_1|$  of two optical modes can be produced. From Eq. (2.3), the fiber dispersion effect can be treated as the constant phase shift  $\theta_D$  and does not cause any influence on the detected beat signal power level, while the intensity-modulated light experiences the periodic signal power suppression as discussed in Fig. 1.3.

Because two optical phases,  $\Phi_1$  and  $\Phi_2$ , of two independent optical modes are usually uncorrelated, however, the linewidth of the produced electrical beat signal becomes as broad as the sum of the linewidths of two optical modes. It is typically of several MHz when using semiconductor laser diodes as optical sources. The beat signals

having broad linewidth are not suitable for the use of various data modulation formats in practical wireless applications. In order to obtain the beat signal with narrow linewidth, the optical phases,  $\Phi_1$  and  $\Phi_2$ , of two independent optical modes should be well correlated each other. For this purpose, there have been typical studies, such as single sideband modulation [16], double-sideband-suppressed carrier modulation [17], optical phase-locked loop [18], and sideband injection locking [19]. In this dissertation, the sideband injection locking method is employed for the optical LO generation, whose characteristics are discussed in more details in Sec. III.

### **A. Optical Single-Sideband Modulation**

The optical single-sideband modulation using a dual-electrode Mach-Zehnder intensity modulator is shown in Fig. 2.1, where the RF-signal at  $\omega_{LO}$  is applied to both electrodes of the Mach-Zehnder modulator. The  $\pi/2$  phase-shifted RF-signal is applied to one electrode. One electrode is dc-biased, while the other electrode is grounded. This optical single-sideband modulator can be modelled as two phase modulators in parallel and its normalized output can be written by [16]:



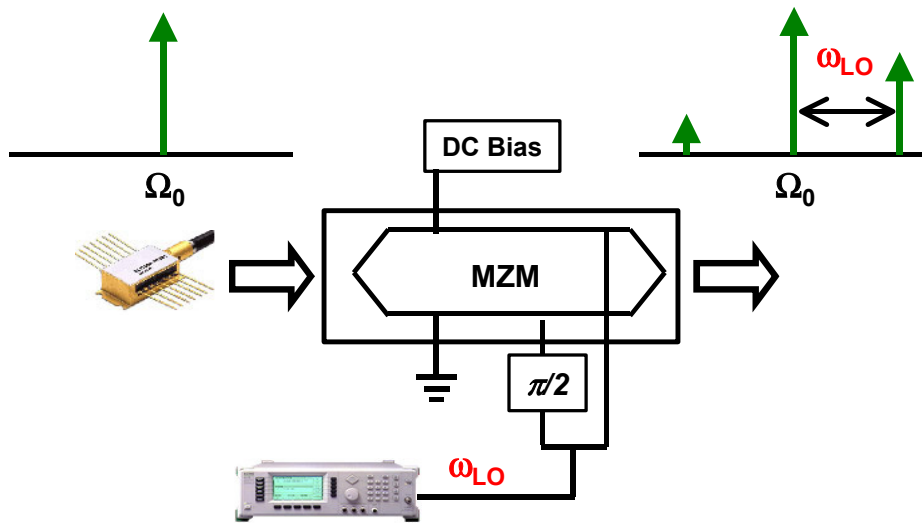


Fig. 2.1. Optical single-sideband modulation using a dual-electrode Mach-Zehnder intensity modulators.

$$E(t) = \frac{\sqrt{P_0}}{2} [\cos(\Omega_0 t + \varepsilon\pi + \alpha\pi \cos \omega_{LO} t) + \cos(\Omega_0 t + \alpha\pi \sin \omega_{LO} t)], \quad (2.4)$$

where  $P_0$  is the average optical power,  $\Omega_0$  the angular frequency of the center optical carrier,  $\varepsilon = V_{DC}/V\pi$  the normalized DC-bias level, and  $\alpha = V_{AC}/V\pi$  the normalized modulation level. For  $\varepsilon = 1/2$  or the quadrature point, Eq. (2.4) can be developed into a Bessel series:

$$E(t) = \frac{\sqrt{P_0}}{2} [J_0(\alpha\pi)\cos\Omega_0 t - J_0(\alpha\pi)\sin\Omega_0 t - 2J_1(\alpha\pi)\cos(\Omega_0 - \omega_{RF})t] \quad \text{with } \alpha < 1/\pi. \quad (2.5)$$

Eq. (2.5) shows clearly that the optical single-sideband modulator produces only two spectral components: one optical center carrier at  $\Omega_0$  and one sideband separated by  $\omega_{LO}$  in the optical spectrum. The complete suppression of the other sideband at  $\Omega_0 + \omega_{LO}$  can be theoretically achieved. One may suppress the sideband at  $\Omega_0 - \omega_{LO}$  in Eq. (2.5) rather than one at  $\Omega_0 + \omega_{LO}$ , if the  $\pi/2$  phase-shifted RF-signal is applied to the different electrode in Fig. 2.1. In addition, because two optical modes at  $\Omega_0$  and  $\Omega_0 - \omega_{LO}$  (or,  $\Omega_0 + \omega_{LO}$ ) are originated from the same optical source, their optical phases are well

correlated. Therefore, the low phase-noise beat signal at  $\omega_{LO}$  in photo-detection can be obtained without any helps of complex electrical feedback circuits.

This single-sideband modulation, however, has several problems. It is very sensitive to the modulator DC-bias level. For the higher  $\omega_{LO}$ , it should need a phase-locked electrical oscillator and high-speed dual-electrode Mach-Zehnder modulator operating at  $\omega_{LO}$ . Thus, the modulator bandwidth can impose a limitation on the accessible LO frequency range.

## B. Double Sideband-Suppressed Carrier Modulation

Using a high-speed Mach-Zehnder intensity modulator, two optical modes with the desired LO frequency separation  $f_{LO}$  can be obtained. The electric-field response of the Mach-Zehnder modulator can be given by: [17]

$$E_{out}(t) = E_{in}(t) \cdot \cos\left[\frac{\pi}{2} \frac{V_{mod}(t)}{V_{\pi}}\right] \cdot \cos(\Omega_0 t) \quad (2.6)$$

where  $E_{in}(t)$  represents the input optical field intensity incident on the

modulator,  $V_{mod}(t)$  the input electrical voltage applied to the modulator and  $\Omega_0$  the angular frequency of optical carrier. When the modulator is RF-modulated at  $\omega_{LO}/2$ , its normalized output electric-field is represented by:

$$V_{mod}(t) = V_{\pi} \cdot (1 + \varepsilon) + \alpha \cdot V_{\pi} \cos\left(\frac{1}{2}\omega_{LO}t\right) \quad \text{and} \quad (2.7)$$

$$\hat{E}_{out}(t) = \frac{E_{out}}{E_{in}} = \cos\left\{\frac{\pi}{2}\left[(1 + \varepsilon) + \alpha \cos\left(\frac{1}{2}\omega_{LO}t\right)\right]\right\} \cdot \cos(\Omega_0 t), \quad (2.8)$$

where  $\alpha$  represents the normalized modulation level and  $\varepsilon$  the normalized bias. The output electric-field in Eq. (2.8) can be re-written as a Bessel series:

$$\begin{aligned} \hat{E}_{out}(t) = & \frac{1}{2}J_0\left(\alpha\frac{\pi}{2}\right) \cdot \cos\left[\frac{\pi}{2}(1 + \varepsilon)\right] \cdot \cos(\Omega_0 t) \\ & - \frac{1}{2}J_1\left(\alpha\frac{\pi}{2}\right) \cdot \sin\left[\frac{\pi}{2}(1 + \varepsilon)\right] \cdot \cos\left(\Omega_0 t \pm \frac{1}{2}\omega_{LO}t\right) \\ & + \frac{1}{2}J_2\left(\alpha\frac{\pi}{2}\right) \cdot \cos\left[\frac{\pi}{2}(1 + \varepsilon)\right] \cdot \cos(\Omega_0 t \pm \omega_{LO}t) \\ & - \frac{1}{2}J_3\left(\alpha\frac{\pi}{2}\right) \cdot \sin\left[\frac{\pi}{2}(1 + \varepsilon)\right] \cdot \cos\left(\Omega_0 t \pm \frac{3}{2}\omega_{LO}t\right) + \dots \quad (2.9) \end{aligned}$$

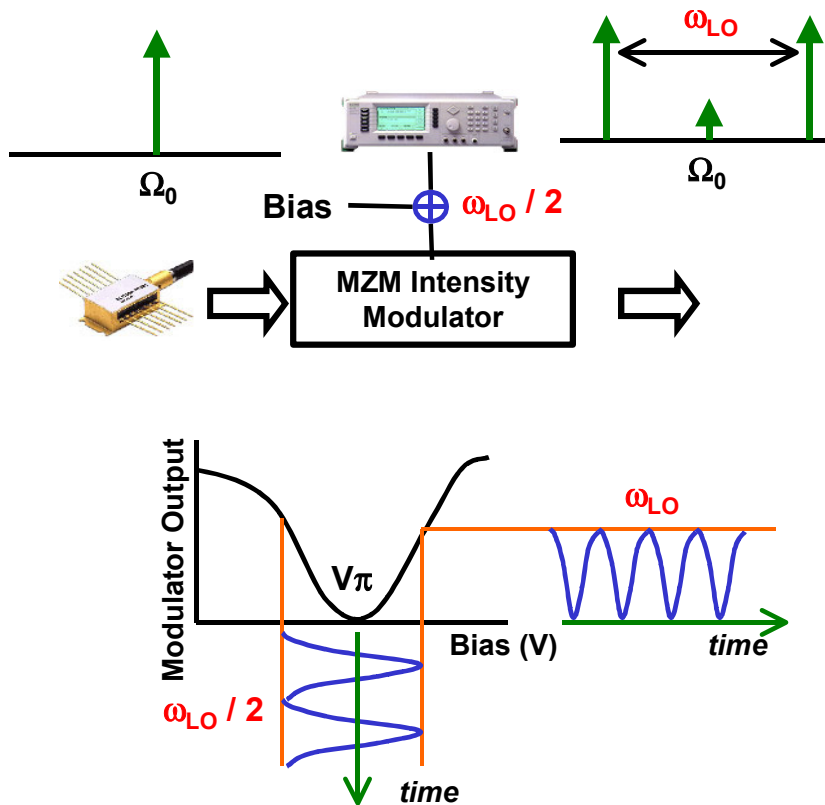


Fig. 2.2. Double sideband-suppressed carrier modulation using Mach-Zehnder intensity modulators.

When  $\varepsilon = 0$  in Eq. (2.9), the DC bias term in  $V_{mod}$  is of  $V_\pi$  and the center optical carrier component is ideally eliminated as described in Fig. 2.2. The second terms of the modulator output at  $\Omega_0 \pm \frac{1}{2}\omega_{LO}$  in Eq. (2.9) become the dominant optical modes having desired frequency separation by  $\omega_{LO}$ . Because the center optical carrier is suppressed, it is called “double sideband-suppressed carrier (DSB-SC)” modulation. Because two optical modes at  $\Omega_0 \pm \frac{1}{2}\omega_{LO}$  comes from the same optical source, their optical phases are well correlated. Thus, the low phase-noise beat signal at  $\omega_{LO}$  in photo-detection can be obtained without any helps of additional electrical feedback circuits. This modulation method, however, requires an additional optical amplifier in implementation since the modulator should be biased at  $V_\pi$  for its output to be minimum in operation as described in Fig. 2.2.

### C. Optical Phase-Locked Loop (OPLL)

In the OPLL scheme of Fig. 2.3, two optical sources are used to produce a beat signal at the desired LO frequency as discussed in Eq. (2.3). If their optical phases are not synchronized or well correlated, the beat signal will have the linewidth as broad as the sum of the linewidths

of two optical sources, master and slave lasers, here. In order to achieve the beat signal with a narrow linewidth, the OPLL employs an electrical feedback circuit as illustrated in Fig. 2.3. Some of optical powers are tapped off and photo-detected in a PD. The phase-comparison between the photo-detected beat signal  $\theta_{PD}$  and the electrical reference oscillator  $\theta_{LO}$  having a narrow linewidth are made by using a microwave mixer as phase-detector. The resulting phase error signal  $\theta_e$  is filtered with the loop filter and used instantaneously to tune the slave laser  $\theta_S$  for  $|\theta_{PD} - \theta_{LO}| = \text{constant}$ . For this, the frequency-offset between two laser  $|\omega_M - \omega_S|$  should be equal to the frequency of the electrical reference oscillator  $\omega_{LO}$ . Thus, the OPLL system can produce the beat signal of two lasers at  $\omega_{LO}$  having the narrow linewidth.

The OPLL system, however, is very complicated for the practical realization because of the loop bandwidth and loop propagation delay. For the stable operation of the OPLL, the wide loop bandwidth as well as the short propagation loop delay are required. For this, the lasers having narrow linewidths should be integrated in one package [18].

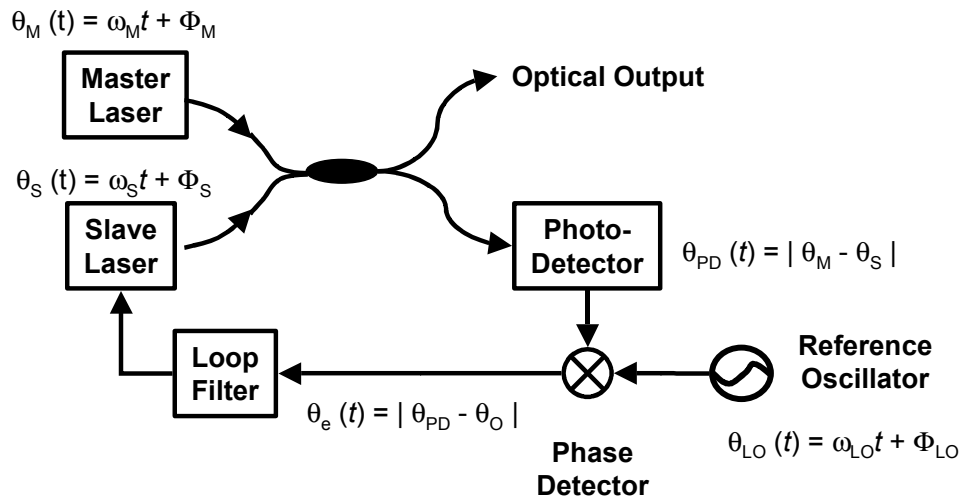


Fig. 2.3. Block diagram for optical phase-locked loop



#### D. Sideband Injection-Locking

The sideband injection-locking method can be used for optically generating micro/millimeter-wave signals. It can easily produce very high frequency signals with low phase noises. There are several experimental demonstrations for this method [3, 19-21] and Braun *et al.* have successfully generated millimeter-wave signals in the 60-GHz range for fiber radio mobile communication applications [3, 20]. Fig. 2.4 shows the operational principle of the sideband injection-locking technique. When a DFB laser acting as master laser (ML) is directly RF-modulated at  $\Omega_m$ , it is intensity-modulated as well as frequency-modulated because of frequency chirp [8, 22-24]. Thus, the ML under RF-modulation produces multiple sidebands that have the frequency separation of the RF-modulation frequency  $\Omega_m$  as illustrated in Fig. 2.4. Two of these sidebands having the target frequency separation are used to injection-lock two separate DFB lasers acting as slave lasers (SLs). Two injection-locked SLs have the target frequency separation, and are synchronized to each other since they are both locked to the same ML.

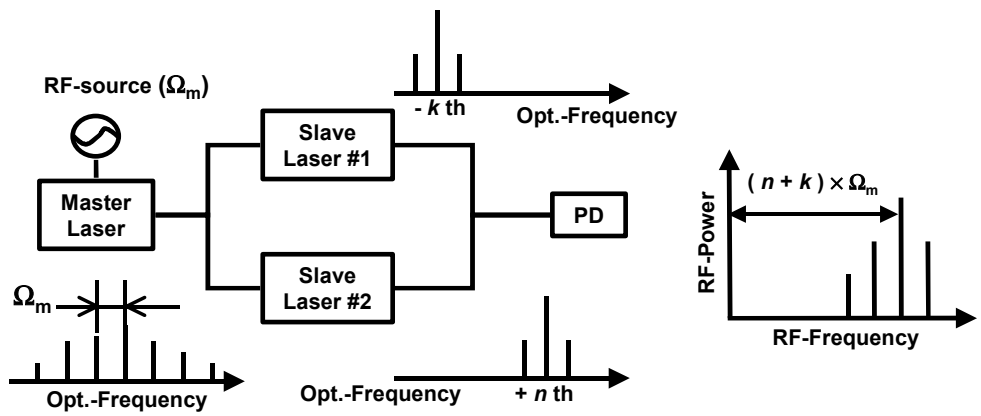


Fig. 2.4. Block diagram for the optical micro- / millimeter-wave generation with sideband injection-locking.

When the output lights from two SLs beat each other in a PD, the desired micro/millimeter-wave signal is generated that have the target frequency and very small phase noise.

Fig. 2.5 shows the measured optical spectra of the optically generated 60-GHz LO source using the sideband injection locking configuration, where the ML is directly RF-modulated at 10 GHz. The multiple sidebands with the 10-GHz separation are produced off from the center ML wavelength around 1552.5nm. For the 60-GHz optical LO source,  $\pm 3$  ML sideband powers get maximized by controlling the RF-modulation level, and is used to injection-lock two slave lasers as shown in Fig. 2.5. When these SL outputs are photo-detected, the stable and low phase-noise 60-GHz LO source is obtained with single sideband phase-noise of about  $-90$  dBc/Hz at 100 kHz frequency-offset as shown in Fig. 2.6. In particular, the phase-noise of the optically generated 60-GHz LO signal follows the ideal multiplication law, or  $20 \times \log_{10} M$ , where  $M$  is the multiplication factor. The minor phase-noise degradation at the offset frequency over 100 kHz is believed to be due to the imperfect physical path-length match between ML and SLs.

Fig. 2.7 shows the changes in the RF-powers and phase-noises of the detected LO source over 6 hours. The variation of the detected LO source powers is confined within  $\pm 0.5$  dB. This minor variation is

believed to be due to the coherence effect between the reflected ML fields from two SLs [25]. The single-sideband phase-noises of the LO source are maintained around  $-90$  dBc/Hz at 100 kHz frequency-offset over measurements. Fig. 2.7 confirms experimentally that the stable and low phase-noise LO source can be achieved with the sideband injection locking scheme.

The OPLL of Sec. II-C and sideband injection locking systems can commonly obtain the desired LO sources realized as beat signals between two lasers. In the OPLL systems, the optical phases of two lasers get synchronized or well correlated at the cost of the complex electrical feedback circuits due to the short loop propagation delay. The sideband injection locking, however, does not require any electrical feedback circuitry. But, the SL lasing frequency should be carefully controlled with laser injection current and temperature in order for the SL to be stable-locked to the desired ML sideband due to the narrow locking range. In order to overcome these problems, the optical injection phase-lock loop system has been recently demonstrated, where it can allow the considerable loop propagation delay in the OPLL system and the wide SL locking range in the sideband injection locking [25, 26].

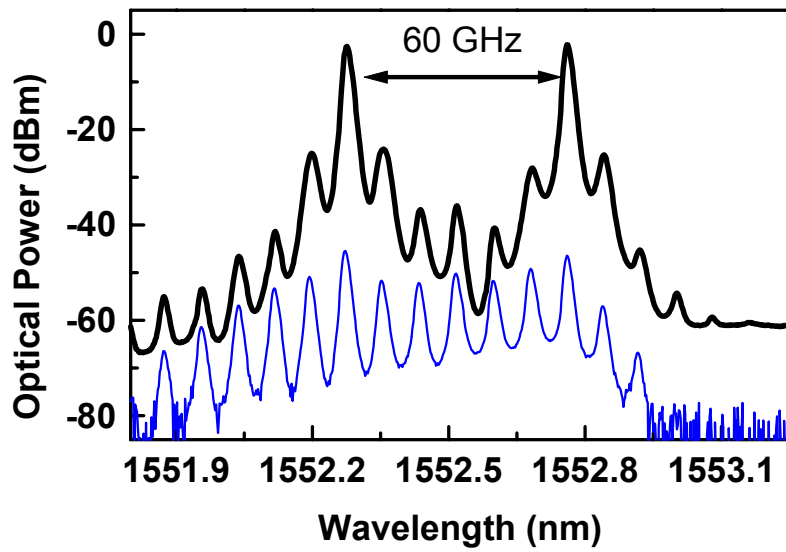
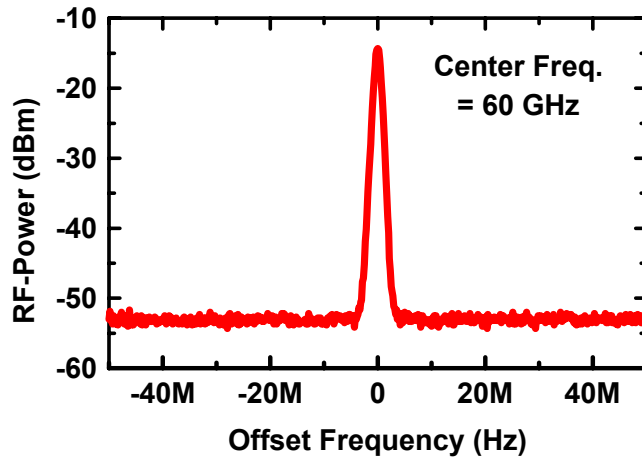
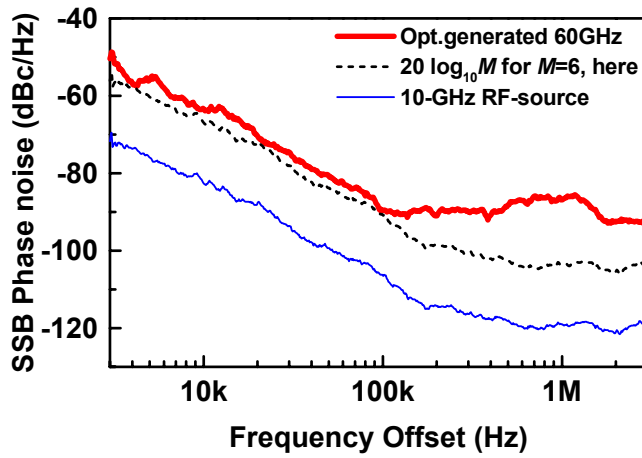


Fig. 2.5. Optical spectra of the RF-modulated ML (thin) and two slave lasers (bold) injection-locked to  $\pm 3$  ML sidebands.

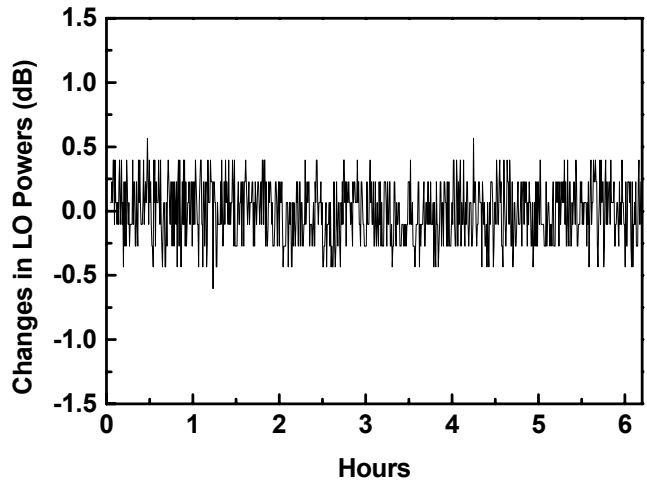


(a)

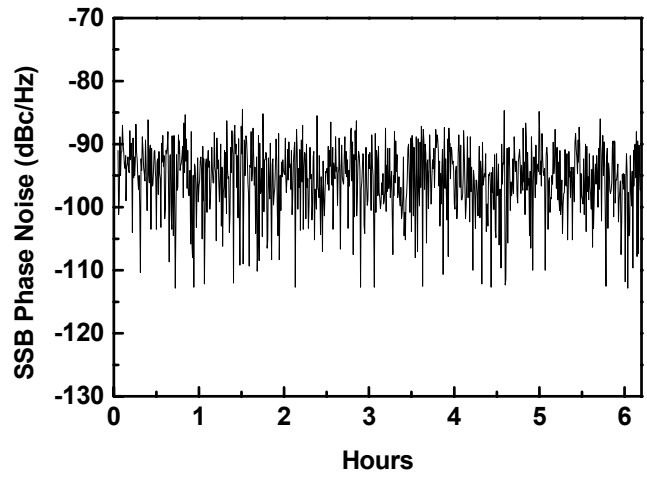


(b)

Fig. 2.6. RF-spectrum (a) and single sideband phase-noise (b) of the 60-GHz beat signals between two injection-locked slave lasers in Fig. 2.4.



(a)



(b)

Fig. 2.7. Long-term intensity variations (a) and single-sideband phase-noises at 100 kHz offset frequency (b) of the LO source generated with sideband injection locking.

### III. Characteristics of Sideband Injection Locking

In the sideband injection-locking scheme, it is often the case that the ML modulation frequency is a sub-harmonic of the desired beat frequency. It can significantly reduce the required ML bandwidth and the operating frequency for the RF source. For example, Braun *et al.* used 3.2-GHz phase-locked electrical oscillator in order to generate 64 GHz beat signals [3, 20]. Consequently, a careful control in the SL lasing frequencies and the amount of ML light injected to SL is required in order to have each SL locked to the desired sideband. When the SL is injection-locked to a certain sideband, the presence of adjacent sidebands that are not involved in injection-locking can influence the spectral characteristics of the resulting beat signals [27, 28]. The presence of undesired beat signals is graphically shown in Fig. 2.4. Since these undesired beat signals can have significant influence on the overall system performance, it is necessary to analyze the characteristics of the undesired beat signals. In this section, the characteristics of the undesired beat signals are discussed numerically and experimentally.



### ◆ Extended Lang's Rate-equations

To a first approximation, the normalized electric field of an RF-modulated ML can be expressed as [22-24]

$$\tilde{E}^{ML}(t) = S_{ML}^{1/2} [1 + m_{IM} \cos(\Omega_m t + \Phi_{IM})]^{1/2} e^{jm_{FM} \sin(\Omega_m t + \Phi_{FM})}, \quad (3.1)$$

where  $S_{ML}$  is the average ML photon density,  $\Omega_m$  the angular modulation frequency,  $m_{IM}$  and  $m_{FM}$  are intensity-modulation (IM) and frequency-modulation (FM) indices, and  $\Phi_{IM}$  and  $\Phi_{FM}$  are the optical phases for IM and FM, respectively. Eq. (3.1) can be rewritten by a Bessel series as follows,

$$\begin{aligned} \tilde{E}^{ML}(t) &= S_{ML}^{1/2} \sum_{k=-\infty}^{\infty} \left[ J_k(m_{FM}) + \frac{m_{IM}}{4} (J_{k+1}(m_{FM}) e^{j\Delta\Phi} + J_{k-1}(m_{FM}) e^{-j\Delta\Phi}) \right] \cdot e^{jk(\Omega_m t + \Phi_{FM})} \\ &= \sum_{k=-\infty}^{\infty} E_k^{ML} \cdot e^{jk\Omega_m t}, \end{aligned} \quad (3.2)$$

where

$$E_k^{ML} = S_{ML}^{1/2} \cdot e^{jk\Phi_{FM}} \cdot \left[ J_k(m_{FM}) + \frac{m_{IM}}{4} (J_{k+1}(m_{FM}) e^{j\Delta\Phi} + J_{k-1}(m_{FM}) e^{-j\Delta\Phi}) \right].$$

$\Delta\Phi$  is the optical phase difference between  $\Phi_{FM}$  and  $\Phi_{IM}$ . In the above equation,  $J_{-k}(m_{FM}) = (-1)^k J_k(m_{FM})$  is used. Eq. (3.2) shows that the RF-modulated ML has multiple sidebands in the optical spectrum that are separated by  $\Omega_m$ .

The characteristics of the SL into which RF-modulated ML light is injected can be modeled by extending Lang's rate-equations [29] in the following manner.

$$\frac{dE_k}{dt} = \frac{1}{2} \left( \Gamma G(N) - \frac{1}{\tau_p} \right) \cdot (1 - j\alpha) \cdot E_k + j(\omega_k^{ML} - \omega^{fr}) \cdot E_k + 2K_C E_k^{ML}, \quad (3.3)$$

$$\frac{dS_u}{dt} = \left( \Gamma G(N) - \frac{1}{\tau_p} \right) \cdot P_u + \Gamma \beta \frac{N}{\tau_n}, \quad (3.4)$$

$$\frac{d\Phi_u}{dt} = \frac{1}{2} \alpha \left( \Gamma g_0(N - n_t) - \frac{1}{\tau_p} \right), \quad (3.5)$$

$$\frac{dN}{dt} = \frac{I}{qV_a} - G(N) \cdot \left( P_u + \sum_k |E_k|^2 \right) - \frac{N}{\tau_n}, \quad (3.6)$$

$$G(N) = \frac{g_0(N - n_t)}{1 + \varepsilon S}, \quad \text{and} \quad S = P_u + \sum_k |E_k|^2.$$

In the above equations,  $E_k$  represents the normalized complex electric field that is locked to the  $k$ -th ML sideband whose normalized complex electric field and angular frequency are denoted by  $E_k^{ML}$  and  $\omega_k^{ML}$ , respectively.  $|E_k|^2$  corresponds to the locked normalized photon density for the  $k$ -th ML sideband.  $\omega^{fr}$  is the lasing angular frequency for the

free-running SL (no light injection).  $S_u$  and  $\Phi_u$  are the unlocked normalized photon density and the optical phase, respectively. The Langevin noise terms are not included in the above equations. The coupling rate ( $K_C$ ) is defined as  $v_g/2L$ . The value of 141.7 GHz is used for  $K_C$  in investigation, which corresponds to the SL cavity length ( $L$ ) of 300  $\mu\text{m}$ . Other parameters have the usual meanings. For calculations, laser diode parameters given in [30] are used.

These extended rate-equations can include the arbitrary number of the ML sidebands, whereas Lang's model in [29] deals with the SL under the single mode laser injection, that is, only one value for  $k$  is considered in the above equations. The field amplitude of the  $k$ -th ML sideband ( $E_k^{ML}$ ) is determined from  $m_{FM}$  that is directly related to the intrinsic laser frequency chirp characteristics. The ML field at the center lasing frequency is denoted by  $E_0^{ML}$ . The negative (positive) sign for  $k$  means that the sideband is located at the lower (higher) frequency than the center frequency ( $k = 0$ ). The angular frequency of the  $k$ -th ML sideband ( $\omega_k^{ML}$ ) can be simply expressed as  $\omega_k^{ML} = \omega_0^{ML} + k \times \Omega_m$ .

## ◆ Simulation Results

For the numerical simulation, it is assumed that three identical semiconductor lasers are used for one ML and two SLs. It is also assumed that the ML is biased at  $1.57 \times I_{th}$  and is RF- modulated at 8 GHz with the modulation current  $I_m$  of  $0.75 \times I_{th}$ . The modulation indices  $m_{IM}$  and  $m_{FM}$  can be calculated for the given condition using linearized laser rate-equations. With these, the ML optical spectrum has  $\pm 2$  ML sideband larger than other sidebands to be the target sidebands for injection-locking two SLs for the beat signal of  $4 \times \Omega_m$  or 32-GHz here. The total of 17 ML sidebands including the center optical mode are considered in calculations. Under these conditions, the effects of the unselected sidebands on the spectral characteristics of the beat signal are investigated at different ML injection powers. The path length differences between ML and two SLs, and between SLs to PD are not considered in calculation, which can cause the relative optical phase deviation and influence the linewidths or phase-noises of the beat signals [3]. The PD is simply assumed an ideal square-law device for the incident optical field.

The frequency locking-range within which SL is locked to the  $k$ -th ML sideband can be analytically given as [31]

$$|\Delta f_k| \leq \frac{K_C}{2\pi} \sqrt{\frac{|E_k^{ML}|^2}{S}} (1 + \alpha^2) \quad (3.7)$$

where  $\Delta f_k$  represents the SL lasing frequency-detuning off from the  $k$ -th ML sideband. Eq. (3.7) shows that the locking range can be widened with the increase of the injected ML light intensity. This locking range can be further classified into two distinctive regimes: stable-locking and unstable-locking. In the stable-locking regime, the output power converges to a steady-state value when a small perturbation is introduced. In the unstable locking regime, however, the power does not converge to the steady-state value but experiences a self-sustained oscillation or even chaos when a small perturbation is introduced. When the single mode ML light is assumed, the stable-locking range can be easily determined from the s-domain stability analysis of the linearized Lang's rate-equations. When two and more ML lights are simultaneously injected to SL, the stable locking range cannot be obtained easily from the s-domain stability analysis since ML lights competes each other to get more optical gains. This is well studied in [32], and is not discussed in further details, here.

In order to consider the influence of the several sidebands on the

stable-locking range, the stable-locking range is determined in the following manner. First, the rate-equations of Eq. (3.3)~(3.6) are numerically solved in time domain with the SL frequency detuned ( $\Delta f_k$ ) in steps of 100 MHz from the  $k$ -th target sideband, where  $\Delta f_k = (\omega_k^{ML} - \omega^{SL}) / 2\pi$ . From the obtained solutions in the time domain, it is judged whether or not the SLs are locked to the  $k$ -th target sidebands by using the following criteria. First, the locked photon density for the  $k$ -th target sideband should be larger than the unlocked photon density, that is,  $|E_k|^2 > S_u$  ( $k = \pm 2$ , here). Second, the locked photon density for the  $k$ -th target sideband should be larger than any other locked photon densities for other sidebands, that is,  $|E_k|^2 > |E_m|^2$  ( $m \neq \pm 2$ , here). Note here that it is possible to have more than one sideband within a particular locking-range. Finally, the relaxation oscillation of the locked photon density should be sufficiently suppressed after reaching the steady state. The suppression ratio should be below -30 dB in this investigation, where

$$\text{suppression ratio} \equiv \frac{\max(|E_k(t)|^2) - \min(|E_k(t)|^2)}{\max(|E_k(t)|^2) + \min(|E_k(t)|^2)} .$$

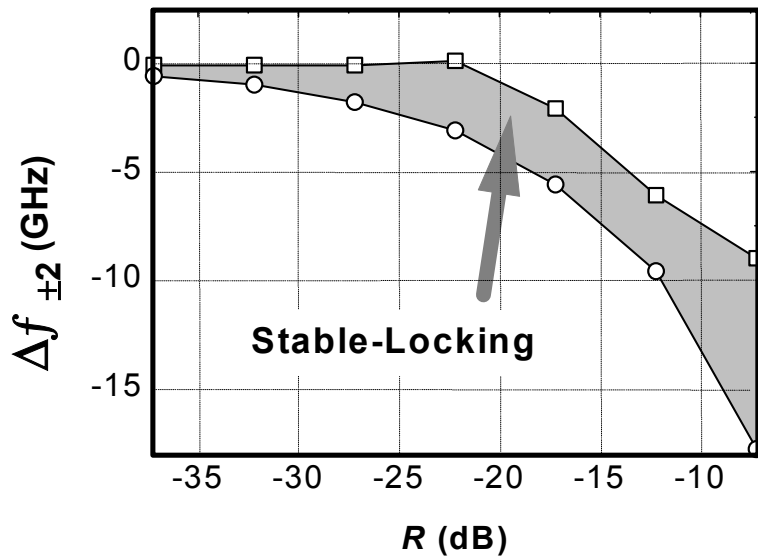


Fig. 3.1. Calculated stable locking range for the  $\pm 2$  target sidebands.

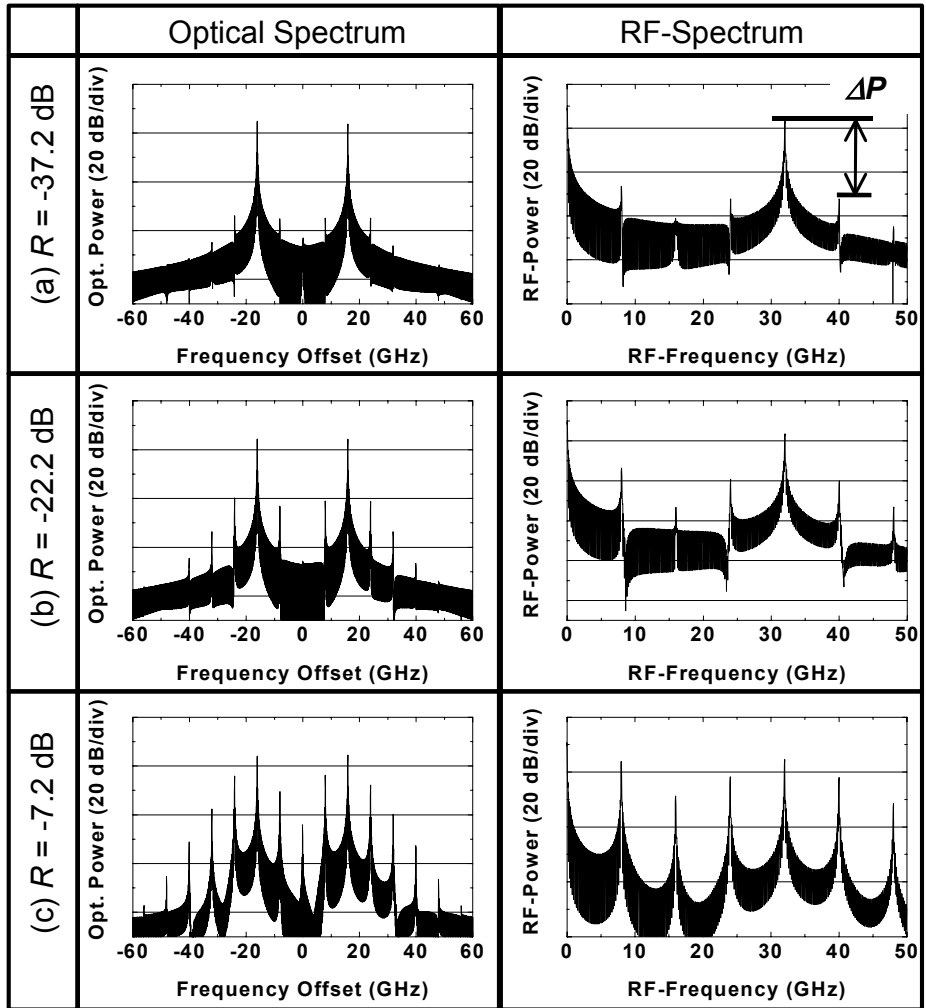


Fig. 3.2. Calculated optical and RF-spectra of the sideband injection-locked SLs for the different  $R$ 's.  $\Delta P$  in the figure indicates the power difference between the desired and undesired adjacent beat signals.



With these, the stable locking-range can be found for the SLs locked to +2 and -2 sidebands at different injection ratios,  $R$ , which is defined as the ratio between the average ML injection power and the free-running SL power. Fig. 3.1 shows the calculated stable locking-range for  $\pm 2$  ML target sidebands. It is found that the center of the stable-locking range is shifted toward lower frequency from the SL lasing frequency as the injection ratio increases. Similar dependence of the stable-locking range on the injection ratio has been studied in [33], whose analysis was given for the semiconductor laser under the CW light injection.

Fig. 3.2 shows the calculated optical and RF-spectra for different values of  $R$ . where the center of the optical frequency axis in the figure represents the ML lasing frequency without modulation. For  $R$  of -37.2 dB in Fig. 3.2-(a), the locking-range is very narrow so that the unselected sidebands are outside the locking range and do not have any significant influence. Consequently, the resulting RF spectrum has undesired beat signals strongly suppressed. For large  $R$  as in Fig. 3.2-(b) and -(c), SLs are frequency-detuned so that they can be stable-locked to the target sidebands. In practice, the frequency-detuning of SL can be done by the control of either laser bias current or laser operating temperature. Most of the SL powers are moved to the target

sideband mode. But, some of the undesired sidebands can also obtain some optical gains from the SLs, since they can be located in the unstable-locking regime. Consequently, with increasing  $R$ , the unwanted sidebands get not strongly suppressed. The resulting RF-spectra have undesired adjacent beat signals whose powers can become comparable to the desired beat signal powers.

Fig. 3.3 shows the power difference ( $\Delta P$ ) between the desired beat signal at 32 GHz ( $P_{32}$ ) and unwanted adjacent beat signal at 40 GHz ( $P_{40}$ ) as function of the injection power ratio. In addition, the bandwidth of the stable-locking range obtained in Fig. 3.1 is also shown for comparison. Small values of  $R$  can suppress the unwanted beat signals strongly but narrow the locking bandwidth. The increase of  $R$  improves the locking bandwidth but degrade the suppression ratio.

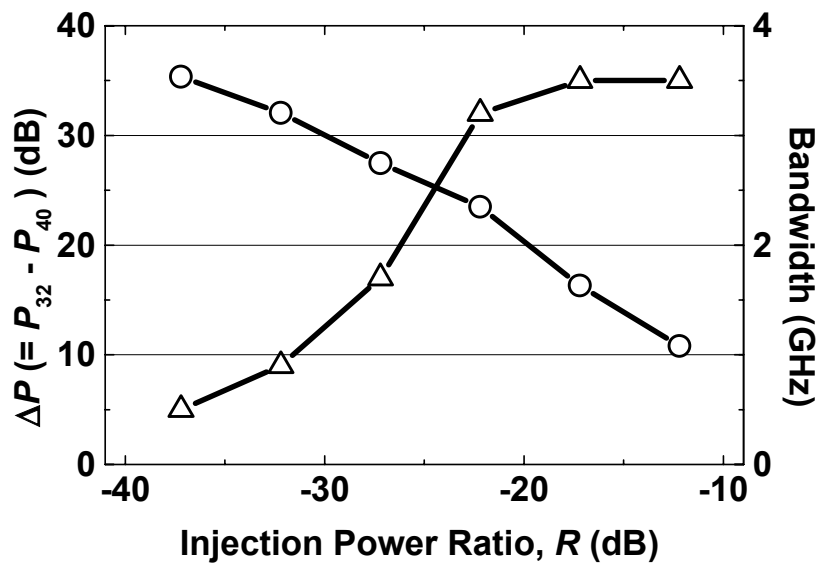


Fig. 3.3. Dependence of  $\Delta P$  (circles) and stable-locking bandwidth (triangles) on  $R$ 's.

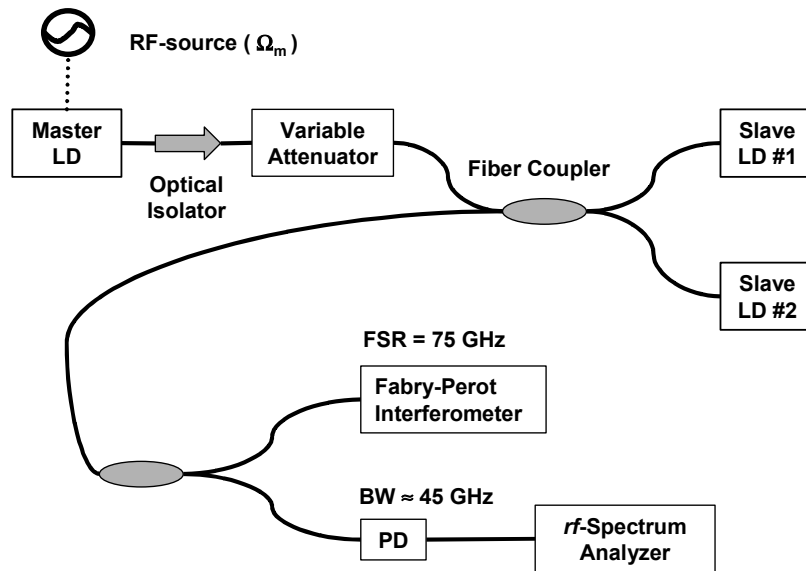
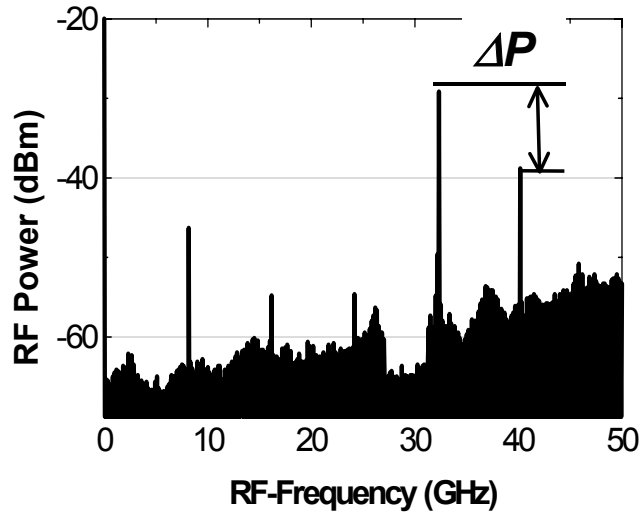


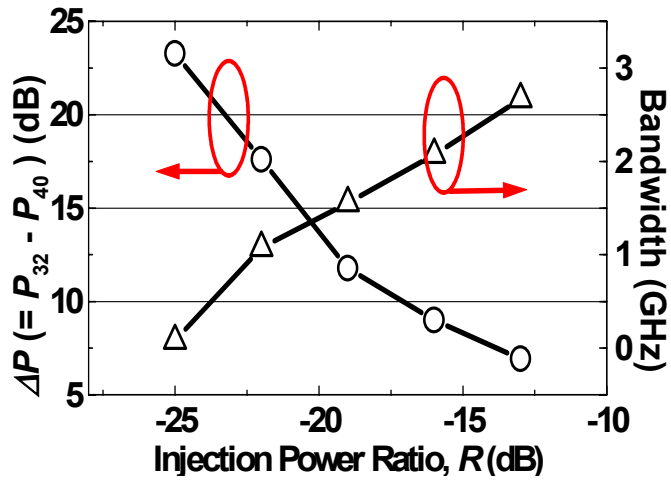
Fig. 3.4. Experimental setup for sideband injection-locking.

## ◆ Experimental Results

Fig. 3.4 shows the setup for experiments performed in order to confirm the simulation results. Three commercial DFB lasers are employed for ML and SLs with the emission wavelength around 1550.2 nm. One isolated DFB-LD used as the ML is biased at  $1.43 \times I_{th}$ . And, Other two unisolated DFB lasers (Samsung SDL24) for the SL's are biased at  $8.1 \times I_{th}$ , emitting about 4 mW. The ML is RF-modulated at 8 GHz to produce the multiple sidebands. In order to make the  $\pm 2$  target sidebands larger than any other ML sideband peaks, the RF-modulation power is adjusted. The ML output with multiple sidebands passes through an isolator and a 3-dB fiber coupler, and is injected into two SLs. Two SL outputs are combined in the fiber coupler. Then, the combined power is divided into two paths. In one path, it is connected to a Fabry-Perot interferometer (FSR = 75 GHz). In the other path, the beat signals produced in a PIN photo-diode (Bandwidth = 45 GHz) are measured by using a RF-spectrum analyzer. Although not illustrated in the figure, a polarization controller is employed in front of each SL so that the coupling efficiency between ML and SL is maximized. A variable optical attenuator is employed in front of the fiber coupler,



(a)



(b)

Fig. 3.5. Measured (a) RF-spectrum for estimated  $R = -16$  dB and, (b)  $\Delta P$  (circles) and stable-locking bandwidth (triangles) for different  $R$ 's.

which adjusts the total injection power into the SLs. In this way, the injection power can be easily changed without adjusting ML bias level or RF modulation power, both of which can affect the IM/FM indices. Under this condition, two SLs are locked to  $\pm 2$  target ML sidebands.

Fig. 3.5(a) shows the measured RF-spectrum generated from the beating of two SLs, each of which is locked to  $\pm 2$  target ML sidebands separated by 32 GHz. The estimated value of  $R$  is about -16 dB. In order to stable-lock SLs to the desired sideband, the SL lasing frequencies are carefully controlled by changing the laser temperature and the bias current.

Fig. 3.5(b) shows the power difference between the desired and undesired RF signals and the stable-locking bandwidth for the different values of  $R$ . The stable-locking bandwidth is determined by carefully measuring the tolerance of the locking condition to the change in SL bias currents. Although the parameters used in simulation do not reflect the lasers used in the experiment, the measured results in Fig. 3.5(b) show qualitatively good agreement with the simulated results shown in Fig. 3.3. These investigation results will provide useful guidelines in the optical high-frequency signal generation using the sideband injection locking for fiber-radio applications.

#### IV. SOA-based Photonic Frequency-Upconverter

The operation principle of SOA-based photonic frequency-upconverter is introduced in Fig. 1.4. The optical LO source has two optical modes with the desired LO frequency separation, which is assumed to be much beyond the SOA gain modulation bandwidth. When the base-band or IF-band data signal and optical LO source are injected simultaneously into a semiconductor optical amplifier, the data signal will modulate SOA carrier density, which in turn can modulate the optical LO source at different wavelength. It is the SOA cross-gain modulation. When the cross-gain modulated optical LO source is photo-detected, the frequency-upconversion of the base-band or IF-band data signal ( $f_{IF}$ ) to lower sideband (LSB,  $f_{LO} - f_{IF}$ ) and upper sideband (USB,  $f_{LO} + f_{IF}$ ) is achieved owing to the PD square-law photo-detection behavior.

Fig. 4.1 is an experimental setup for photonic frequency-upconversion, where the 1-GHz IF-signal and the 25-GHz optical LO source are employed. The optical LO source is produced by the sideband injection-locking method as discussed in Sec. II-D and Sec. III. The SOA (Samsung OA40B3A) used in the experiment has less than 1-dB polarization dependence loss and has, when biased at



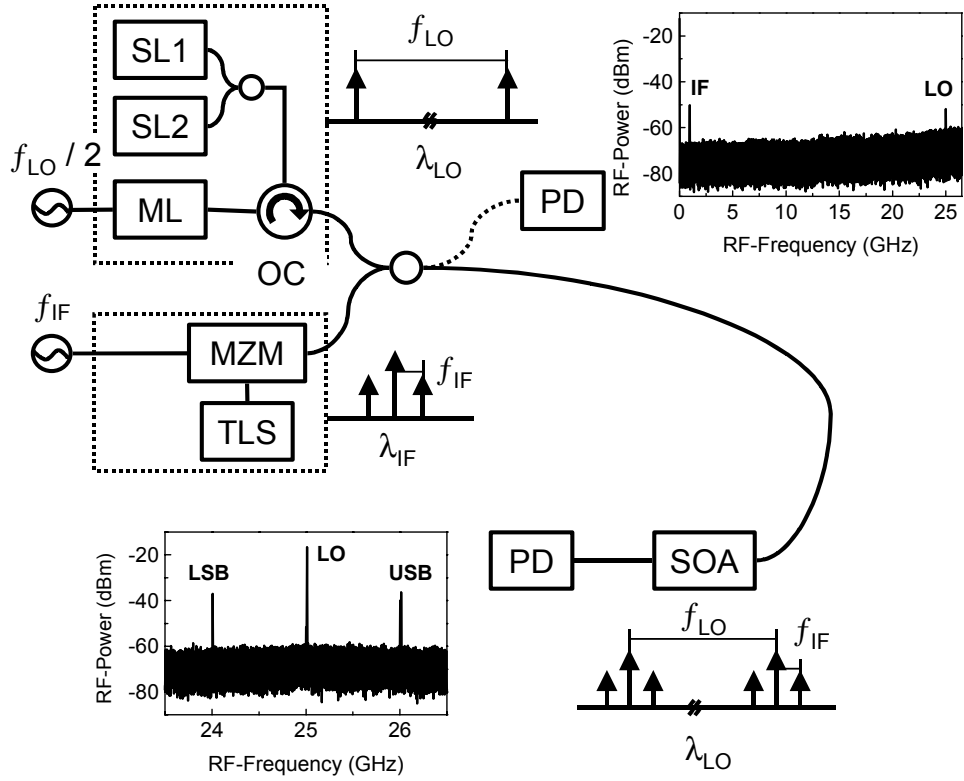


Fig. 4.1. Experimental setup for photonic frequency-upconversion using SOA.

TLS: tunable light source, MZM: Mach-Zehnder intensity modulator, ML: master laser, SL: slave laser, and OC: optical circulator. In the experiment,  $f_{IF} = 1$  GHz, and  $f_{LO} = 25$  GHz.

150 mA, larger than 40 nm of optical gain wavelength range, larger than 5 dBm in output saturation power, and about 3 GHz of gain modulation bandwidth. No polarization control is used. An optical attenuator is placed before PD in order to avoid any non-linear photo-detection effect at the large optical power [13], which may interfere with upconversion process.

Two insets in Fig. 4.1 show the pre-conversion and post-conversion RF-spectra measured before and after SOA, respectively. Two insets show the frequency-upconversion of the 1-GHz IF signal with the 25-GHz optical LO signal to LSB (24 GHz) and USB (26 GHz). In addition, one can find that the post-conversion USB and LSB signal powers are much larger than the pre-conversion IF-signal power before SOA. For the better understanding of this upconversion process, the numerical analysis and experiments are performed.

The numerical analysis is based on the approach given in [34]. When the fields of optical IF signal  $E_{IF}$  and optical LO signal  $E_{LO}$  enter the SOA at  $z=0$ , their propagation in SOA and the change in SOA carrier density can be expressed as:

$$\frac{dE_{IF,LO}}{dz} = \frac{1}{2} \Gamma a_{IF,LO} (N - N_{IF,LO}) E_{IF,LO}, \quad (4.1)$$

$$\begin{aligned}
\frac{dN}{dt} &= \frac{I}{qV} - \frac{N}{\tau_S} - \sum_{i=IF,LO} a_i (N - N_i) \frac{|E_i|^2}{\hbar \omega_i A_{eff}} \\
&= \frac{I}{qV} - \frac{N}{\tau_S} - \sum_{i=IF,LO} (N - N_i) \frac{|E_i|^2}{\tau_S P_i^{sat}}, \tag{4.2}
\end{aligned}$$

where  $a_{IF,LO}$ ,  $N_{IF,LO}$  and  $\omega_{IF,LO}$  are the differential gain, the transparent carrier density and the optical angular frequency for the optical IF and LO signals.  $\Gamma$  is the confinement factor,  $I$  the SOA injection current,  $q$  the electron charge,  $V$  the SOA active volume,  $\tau_S$  the spontaneous carrier lifetime,  $\hbar$  the plank constant, and  $A_{eff}$  the effective mode area.  $P_{IF,LO}^{sat} = A_{eff} \hbar \omega_{IF,LO} / \tau_S a_{IF,LO}$  is defined as the saturation power for the optical IF and LO signals. Four-wave mixing effects between the optical IF and LO signals in SOA are not taken into account for simplicity in analysis. The solution of Eq. (4.1) can be written as

$$E_{IF,LO}(t, z) = E_{IF,LO}(t, z=0) \exp\left\{ \Gamma a_{IF,LO} \left[ \sigma(t, z) - N_{IF,LO} z \right] / 2 \right\}, \tag{4.3}$$

where,  $\sigma(t, z) = \int_0^z N(t, z') dz'$  represents the spatially integrated carrier density. By integrating both sides of Eq. (4.2) with respect to  $z$ ,

one can obtain

$$\frac{d\sigma}{dt} = \frac{Iz}{qV} - \frac{\sigma}{\tau_S} - \sum_{i=IF,LO} \frac{|E_i(t,0)|^2}{\Gamma \hbar \omega_i A_{eff}} \{ \exp[\Gamma a_i (\sigma - N_i z)] - 1 \}. \quad (4.4)$$

When the optical IF signal is harmonically modulated and the optical LO signal has two optical modes separated by  $f_{LO}$  as described in Fig. 4.1,  $E_{IF}$  and  $E_{LO}$  can be written as

$$\begin{aligned} E_{IF}(t, z=0) &= \sqrt{\bar{P}_{IF}} (1 + m_{IM} \cos(\Omega_{IF} t))^{1/2} \cdot e^{-j\omega_{IF} t} \\ &= (\bar{P}_{IF} + \Delta P_{IF} e^{-j\Omega_{IF} t} + \Delta P_{IF}^* e^{j\Omega_{IF} t})^{1/2} \cdot e^{-j\omega_{IF} t}, \end{aligned} \quad (4.5)$$

$$E_{LO}(t, z=0) = \sqrt{\bar{P}_{LO}/2} (e^{-j\Omega_{LO} t/2} + e^{j\Omega_{LO} t/2}) \cdot e^{-j\omega_{LO} t}. \quad (4.6)$$

$\bar{P}_{IF,LO}$  and  $\Omega_{IF,LO} (= 2\pi f_{IF,LO})$  are the average light intensity and the angular electrical modulation frequency for the optical IF or LO signals.

$m_{IF}$  is the intensity modulation index and  $\Delta P_{IF} = \Delta P_{IF}^* = \frac{1}{2} m_{IM} \bar{P}_{IF}$  for relatively small intensity-modulation of the optical IF signal. If we assume that  $f_{LO}$  is much larger than the SOA gain modulation frequency bandwidth, which is the usual case in applications, then only optical IF signals have an influence on the SOA carrier density

modulation with  $\sigma = \sigma_S + \Delta\sigma e^{-j\Omega_{IF}t} + \Delta\sigma^* e^{j\Omega_{IF}t}$ .  $\sigma_S$  is the spatially integrated steady-state carrier density and can be numerically obtained from the steady-state solution of Eq. (4.4), or  $d\sigma/dt = 0$ . From the first-order perturbation of Eq. (4.4), we can obtain

$$\begin{aligned}\Delta\sigma &= -\frac{(G_{IF} - 1)\Delta P_{IF}}{\Gamma\hbar\omega_{IF}A_{eff}(-j\Omega_{IF} + \gamma_{eff})} \quad \text{and} \\ \Delta\sigma^* &= -\frac{(G_{IF} - 1)\Delta P_{IF}^*}{\Gamma\hbar\omega_{IF}A_{eff}(j\Omega_{IF} + \gamma_{eff})}\end{aligned}\quad (4.7)$$

where

$$\begin{aligned}\gamma_{eff} &= 1/\tau_S + 1/\tau_{S_{IF}} + 1/\tau_{S_{LO}} \quad \text{and} \\ \tau_{S_{IF,LO}} &= A_{eff}\hbar\omega_{IF,LO}/G_{IF,LO}a_{IF,LO}\bar{P}_{IF,LO} \\ &= \tau_S P_{IF,LO}^{sat}/G_{IF,LO}\bar{P}_{IF,LO}.\end{aligned}$$

In the above equations,  $\gamma_{eff}$  is the effective recombination rate,

$$G_{IF,LO} = \exp[\Gamma a_{IF,LO} \cdot (\sigma_S - N_{IF,LO} z)]$$

the saturated gain and  $\tau_{S_{IF,LO}}$

the stimulated recombination lifetime for the optical IF or LO signals. Using Eq. (4.7) together with Eq. (4.6), the optical LO signal after SOA

can be written as:

$$\begin{aligned} \tilde{E}_{LO}(t) = & \sqrt{\frac{G_{LO}\bar{P}_{LO}}{2}} \left( e^{-j\frac{1}{2}\Omega_{LO}t} + e^{j\frac{1}{2}\Omega_{LO}t} \right) \cdot e^{-j\omega_{LO}t} \\ & \times \left( 1 + \frac{1}{2}\Gamma a_{LO}\Delta\sigma e^{-j\Omega_{IF}t} + \frac{1}{2}\Gamma a_{LO}\Delta\sigma^* e^{j\Omega_{IF}t} \right). \end{aligned} \quad (4.8)$$

with the approximation of  $e^x \approx 1+x$ . Eq. (3.8) shows that the SOA carrier density modulation by the optical IF signal produces new sidebands at  $\omega_{LO} \pm \left( \frac{1}{2}\Omega_{LO} \pm \Omega_{IF} \right)$  in the spectrum of optical LO signals.

They are the results of the SOA cross-gain modulation, because optical IF signals modulate the SOA carrier density, which in turn modulates optical LO signals at  $\omega_{LO} \pm \frac{1}{2}\Omega_{LO}$ . The photo-detected current after SOA can be obtained from  $\tilde{I}_{LO}^{PD}(t) = R_{PD} \left| \tilde{E}_{LO}(t) \right|^2$  and its USB signal current at  $f = f_{LO} + f_{IF}$  is given as

$$\tilde{I}_{LO}^{PD}(f_{LO} + f_{IF}) = R_{PD} G_{LO} \bar{P}_{LO} \Gamma a_{LO} \Delta\sigma^* / 2,$$

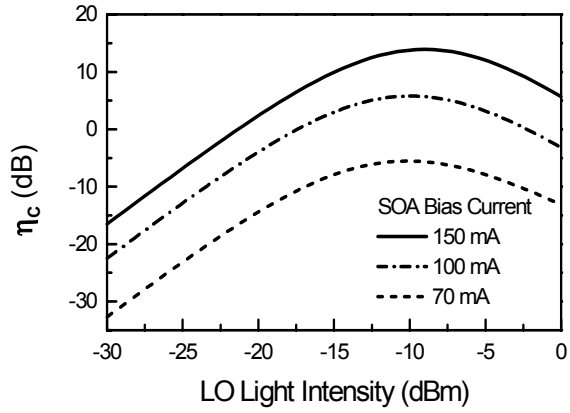
where  $R_{PD}$  is PD responsivity. The photo-detected IF signal current before SOA can be written as  $I_{IF}^{PD}(f_{IF}) = R_{PD} \Delta P_{IF}$  from Eq. (4.5). Then, the frequency-upconversion efficiency in the RF-spectrum can be

derived as

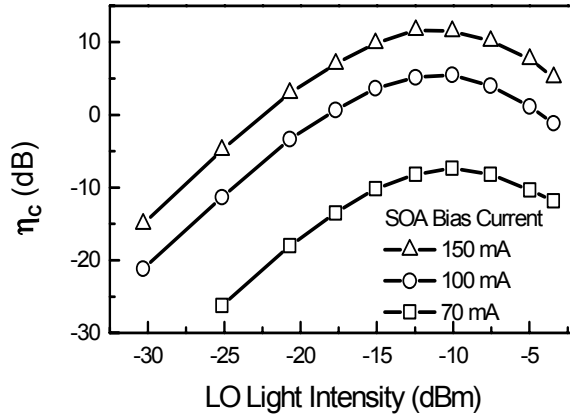
$$\begin{aligned} \eta_C &= \left| \frac{\tilde{I}_{LO}^{PD}(f_{LO} + f_{IF})}{I_{IF}^{PD}(f_{IF})} \right|^2 = \left| \frac{G_{LO} a_{LO} \bar{P}_{LO} (G_{IF} - 1)}{2 \hbar \omega_{LO} A_{eff} (j\Omega_{IF} + \gamma_{eff})} \right|^2 \\ &= \left| \frac{G_{LO} \bar{P}_{LO} (G_{IF} - 1)}{2 \tau_S P_{sat,LO} (j\Omega_{IF} + \gamma_{eff})} \right|^2. \end{aligned} \quad (4.9)$$

Eq. (4.9) shows that the conversion efficiency is proportional to SOA optical gain and LO light intensity. Fig. 4.2(a) shows the calculated results for the frequency-upconversion efficiency at various bias conditions and LO intensities. For calculations, SOA parameters given in [35] are used. The coupling loss of 7dB is assumed for SOA [36].

The conversion efficiency increases initially with LO intensity. But, if LO intensity is too large, the conversion efficiency begins to decrease. This is because the strong LO light will deplete the SOA carriers as shown in Eq. (4.2) and, in turn, saturate the SOA optical gains as. The experimental validation is given in Fig. 4.2(b) where a commercially available SOA (Samsung OA40B3A) is used. Without the knowledge for the numerical values of the parameters for the SOA used in the experiment, it was possible only to make a qualitative



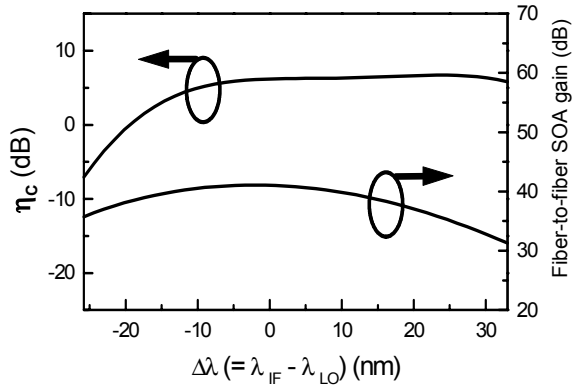
(a)



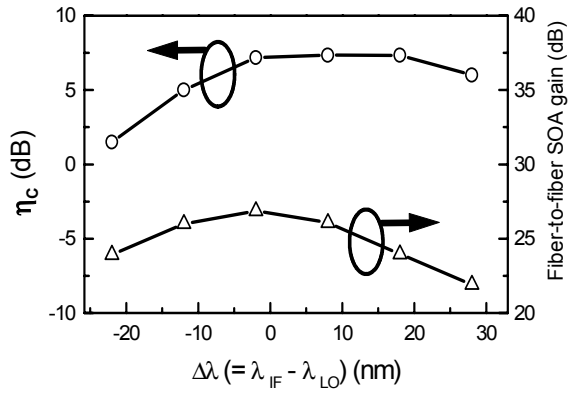
(b)

Fig. 4.2 Calculated (a) and experimental (b) results of signal frequency-upconversion efficiency with LO light intensity for  $\overline{P}_{IF} = -10$  dBm,  $f_{IF} = 1$  GHz,  $f_{LO} = 25$  GHz,  $\lambda_{IF} = 1540$  nm and  $\lambda_{LO} = 1552$  nm.





(a)



(b)

Fig. 4.3. Frequency-upconversion efficiency for different SOA input wavelengths when SOA is biased at 100 mA,  $\bar{P}_{IF} = -10$  dBm,  $\bar{P}_{LO} = -11$  dBm,  $f_{IF} = 1$  GHz and  $f_{LO} = 25$  GHz.  $\lambda_{IF}$  is wavelength-tuned off from  $\lambda_{LO}$  of 1540 nm in calculation (a) and 1552 nm in measurement (b).

comparison at present.

The conversion efficiency can also vary depending on the optical IF and LO signal wavelengths simply because the optical gain in an SOA is wavelength-dependent. Fig. 4.3 shows the calculated and measured frequency-upconversion efficiencies for different IF wavelengths with optical LO wavelength fixed near the SOA gain peak. For comparison, the fiber-to-fiber SOA gain for the SOA light input power of  $-40$  dBm is also shown. As can be predicted by Eq. (4.9), high upconversion efficiencies can be achieved as long as the SOA input wavelengths are within the SOA optical gain bandwidth. In particular, as the optical IF wavelength gets close to the optical gain peak, higher efficiency can be achieved. In Fig. 4.3, the maximum conversion efficiency is achieved at the wavelength slightly longer than the gain peak wavelength for  $-40$  dBm input power. It is because the decreased SOA carrier density by the optical IF and LO signals shifts the optical gain peak toward the longer wavelength.

Eq. (4.9) shows that the effective recombination rate,  $\gamma_{eff}$ , limits the SOA conversion efficiency and thus, the conversion efficiency has an optical IF frequency limit [34]. From Eq. (4.9), the 3-dB modulation frequency for the conversion efficiency can be derived as

$$\begin{aligned}
f_{IF}^{3-dB} &= \frac{1}{2\pi} \gamma_{eff} \\
&= \frac{1}{2\pi \tau_s} \left( 1 + \frac{G_{IF} \bar{P}_{IF}}{P_{IF}^{sat}} + \frac{G_{LO} \bar{P}_{LO}}{P_{LO}^{sat}} \right), \tag{4.10}
\end{aligned}$$

As an example, Fig. 4.4 shows the calculated frequency modulation responses of the conversion efficiency at several SOA bias currents.  $f_{IF}^{3-dB}$  increases with SOA bias currents because it is proportional to the optical gain provided by SOA. In addition, Eq. (4.10) shows that the modulation bandwidth for the IF-signal upconversion can be also improved with the increase of the injected optical IF and LO power levels. The modulation bandwidth for the conversion efficiency cannot be directly given at present due to the experimental environment. But, it can be indirectly estimated, since it corresponds to  $1/\sqrt{3}$  of the 3-dB frequency of the SOA cross-gain modulation.

Fig. 4.5 shows the measurement setup and result for SOA cross-gain modulation response with a network analyzer, where the CW probe signal is gain-modulated by the RF-modulated pump signal in the SOA and is used to measure the SOA modulation bandwidth.

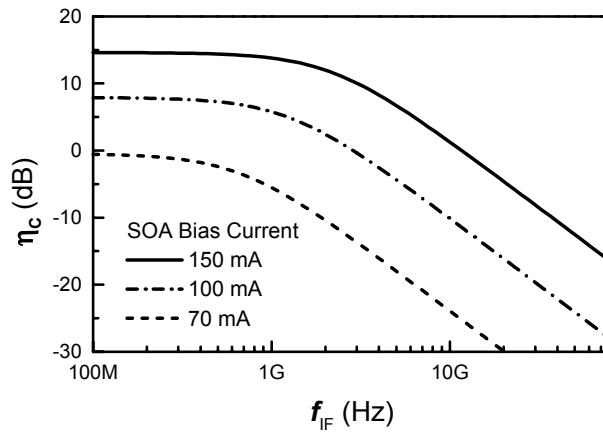


Fig. 4.4. Calculated frequency responses of the frequency-upconversion efficiency for different SOA bias currents when  $\lambda_{LO} = 1552$  nm,  $\lambda_{IF} = 1540$  nm, and  $\bar{P}_{IF} = \bar{P}_{LO} = -10$  dBm.

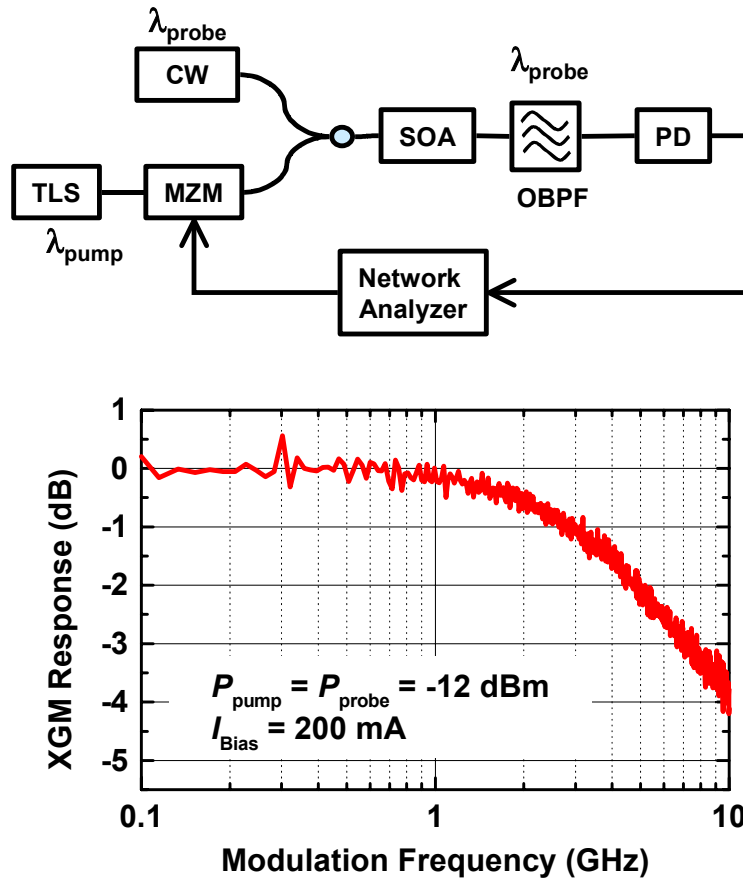


Fig. 4.5. Normalized SOA cross-gain modulation (XGM) response when the SOA is biased at 200 mA. TLS : tunable light source, MZM : Mach-Zehnder intensity modulator, OBPF : optical bandpass filter.

Since the 3-dB frequency of the SOA cross-gain modulation is about 7 GHz from Fig. 4.5, the 3-dB modulation frequency  $f_{IF}^{3-dB}$  of Eq. (4.10) for the conversion efficiency is about 4 GHz. It should be noted that this IF frequency limit for the optical IF signal does not pose any problem in applications, because the typical radio-on-fiber systems have IF frequencies not exceeding the gigahertz range.

The numerical analysis is based on the assumption that the optical LO source has two optical modes with the desired LO frequency separation that is much beyond the SOA gain modulation bandwidth. Thus, the SOA carrier density will not be modulated at the rate of LO frequency at all. Consequently, no matter how high frequency the optical LO source has, the conversion efficiency in Eq. (4.9) should not be affected. In order to verify this assumption, the optical LO source was produced by the double-sideband-suppressed carrier modulation and its frequencies were swept up to 70 GHz from 25 GHz in measuring the conversion efficiencies. As shown in Fig. 4.6, the conversion efficiency gets degraded after 60 GHz, whose frequency is of the nominal photo-detection bandwidth of the high-speed PIN PD (Discovery, DSC10ER) used in measurements. Therefore, the successful frequency-upconversion is possible as long as the LO frequency is within the PD photo-detection bandwidth.

The key characteristics of the proposed photonic frequency-upconversion can be summarized as follows. First, it can be achieved with SOA cross-gain modulation and PD square-law photo-detection. Second, its efficiency is directly attributed by the SOA optical gain and can be optimized by either controlling the optical LO power or selecting the optical IF and LO wavelengths within the SOA optical gain bandwidth. Third, the IF frequency selection is determined by the SOA gain modulation bandwidth, whereas the LO frequency should be within the PD bandwidth. Furthermore, the conversion efficiency would not be much affected by the SOA input light polarization as long as polarization-insensitive SOA is used.

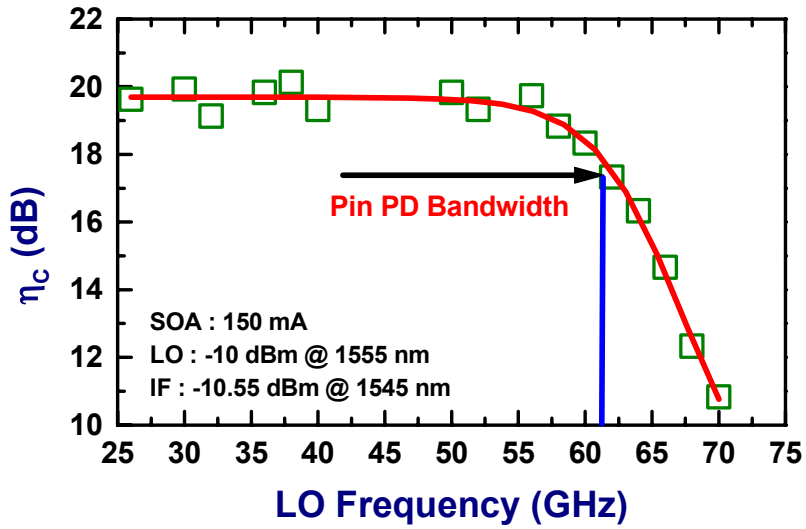


Fig. 4.6. Measured LO frequency responses for  $\bar{P}_{LO} = -10$  dBm at  $\lambda_{LO} = 1552$  nm and  $\bar{P}_{IF} = -10.55$  dBm at  $\lambda_{IF} = 1540$  nm when SOA is biased at 150 mA.



## V. WDM / Radio-on-Fiber Distribution

In the previous section, there has introduced the efficient photonic frequency-upconversion of optical IF signals with optical LO signals using SOA cross-gain and PD square-law photo-detection. It is found that high conversion efficiencies can be obtained by either controlling the optical LO power or selecting the optical IF and LO wavelengths within the SOA optical gain bandwidth. Using these useful features, this section experimentally demonstrates a new distribution scheme of two 622 Mbps base-band digital WDM channels in a 60 GHz radio-on-fiber system. As shown in Fig. 5.1, WDM data are wavelength-selectively distributed to base-stations and one 60 GHz optical LO is shared among base-stations. The optical LO has two optical modes separated by the desired LO frequency of  $f_{LO}$  to avoid dispersion-induced signal suppression as discussed in Sec. II. In the experiment, the 60-GHz optical LO signal is produced by the sideband injection locking method, where two of the sidebands produced by the directly modulated master laser at 10 GHz injection-lock two slave lasers resulting in two dominant optical modes separated by 60 GHz as shown in the optical and RF spectra of Fig. 2.5 and Fig. 2.6, respectively.

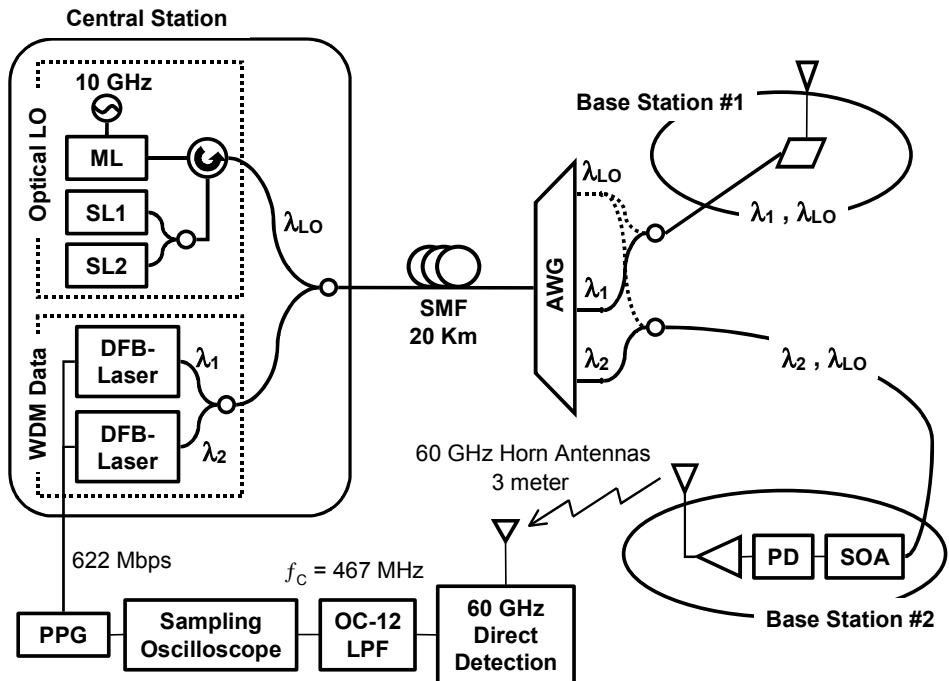
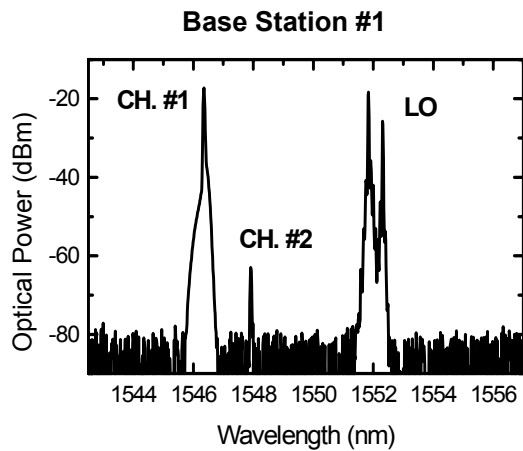
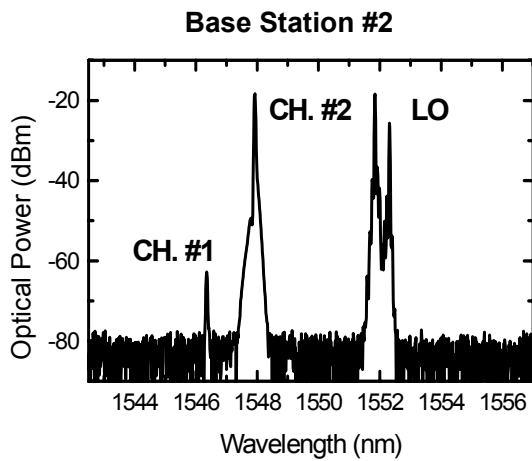


Fig. 5.1. WDM / 60-GHz radio-on-fiber distribution configuration. ML represents master laser, SL slave laser, SMF single-mode fiber, PPG pseudo-random pattern generator and AWG arrayed waveguide grating



(a)



(b)

Fig. 5.2. Measured optical spectra for (a) base station #1 and (b) base station #2 after AWG.

Photonic frequency-upconversion of WDM data signals with optical LO signals are achieved remotely at base stations, which can eliminate the needs for high-frequency electrical mixers and LO sources. Two WDM channels are realized by directly modulating two DFB lasers with 622 Mbps NRZ pseudo-random bit sequence of  $2^{15}-1$  bits and multiplexed with the 60-GHz optical LO signals having different wavelengths. After propagating 20-km long standard single-mode fiber, the WDM data and LO signals are de-multiplexed with an arrayed waveguide grating (AWG) in the wavelength domain. Each WDM channel is delivered to one base station along with the common optical LO signals as shown in Fig. 5.2. The slight suppression of one of the optical LO modes is due to the AWG passband (0.4nm) being narrower than the 60-GHz mode separation (0.48nm).

At the base stations, data signals modulate the SOA carrier density as they co-propagate through an SOA along with optical LO signals. The modulated SOA carrier density, in turn, modulates the optical LO signals. The SOA cross-gain modulation by the optical LO signals is negligible since  $f_{LO}$  of 60 GHz is much beyond the SOA gain modulation frequency bandwidth. When the modulated LO signals are photo-detected in PD, frequency-upconversion of data signals to  $f_{LO}$  is achieved. Fig. 5.3 shows the measured RF-spectrum of the frequency-

upconverted 622 Mbps data with the 60 GHz optical LO signal for base station #2. The spectral asymmetry in Fig. 5.3 comes from the fact that the amplifiers employed in the experiment did not provide flat RF-gains around 60 GHz.

Fig. 5.4(a) shows the measured bit error rate of the upconverted 622 Mbps NRZ data of Fig. 5.3 that is demodulated by direct-detection using a schottky diode and then electrically filtered with a standard OC-12 low pass filter ( $f_c = 467$  MHz). Fig. 5.4(b) is the eye-diagram of the recovered 622 Mbps NRZ data when it meets the BER of  $10^{-9}$ . The PD sensitivity will be further improved if the coherent detection method with an electrical phase lock loop rather than the direct detection as incoherent detection is employed for the demodulation. The frequency-upconverted data signals are re-transmitted over 3-meter in free space using 60 GHz horn antennas. As shown in Fig. 5.5, clear eye-openings are achieved for both base stations.

Although the present demonstration has only two WDM channels, more WDM channels are possible as long as their wavelengths are within the optical gain wavelength bandwidth of SOA used. In addition, by utilizing different IF frequencies for WDM data, different wireless carrier frequencies can be provided to different base stations. This proposed scheme would be useful in radio-on-fiber systems where one

optical LO signal is shared among multiple base stations addressed by their wavelengths.

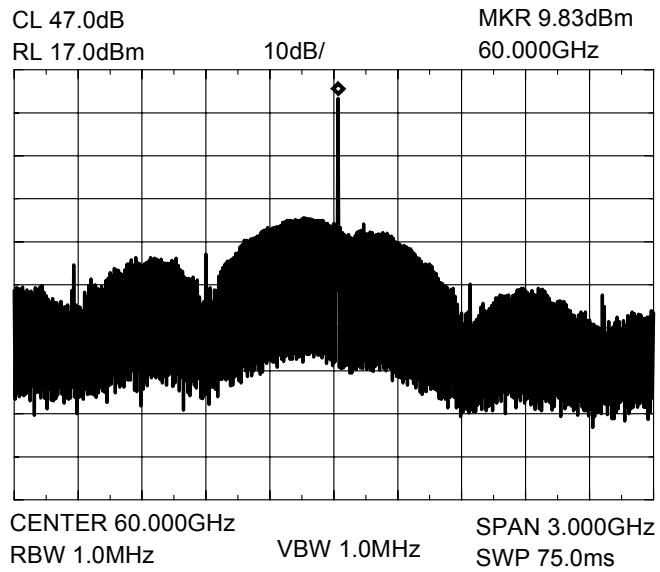
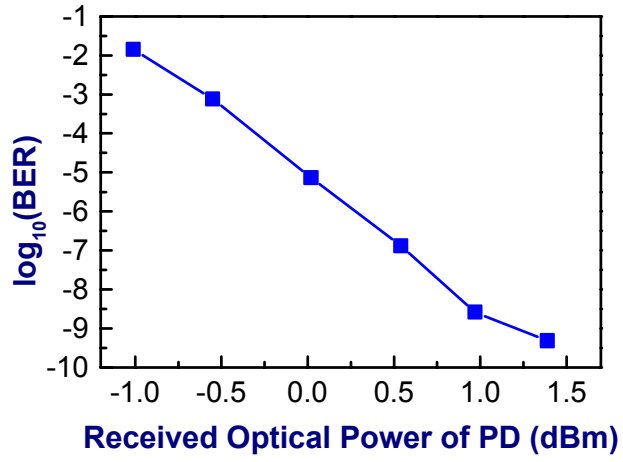
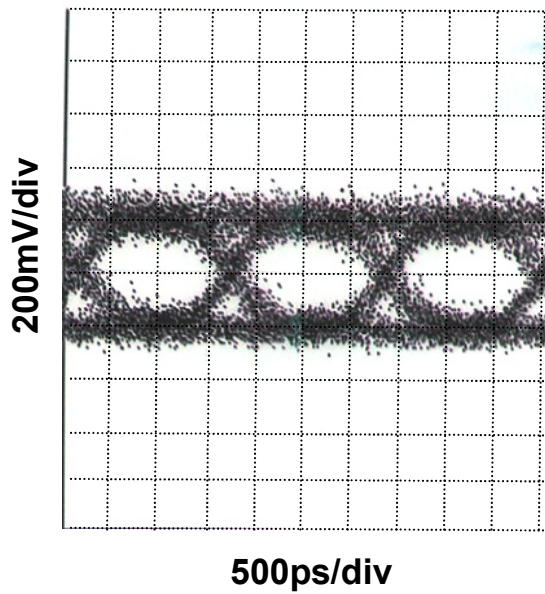


Fig. 5.3. Measured RF-spectrum of frequency-upconverted 622 Mbps data with the 60-GHz optical LO signal for base station #2.



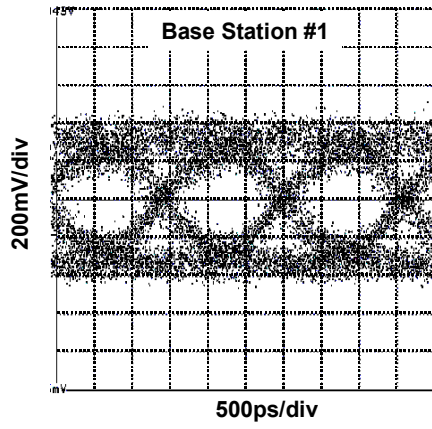
(a)



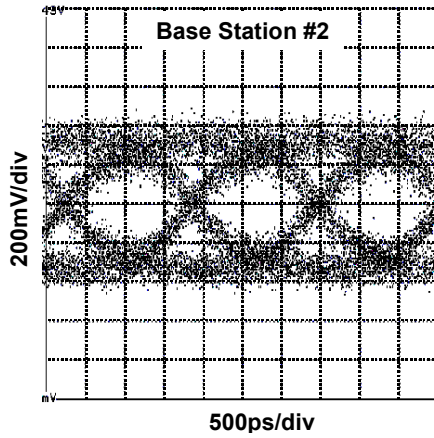
(b)

Fig. 5.4. Bit error rate (a) and eye-diagram (b) of recovered 622 Mbps data after 20-km fiber-optic link in Fig. 5.1.





(a)



(b)

Fig. 5.5. Measured eye-diagrams of recovered 622 Mbps data for (a) base station #1 and (b) base station #2 after 20-km fiber-optic link and 3-meter wireless link shown in Fig. 5.1.

## **VI. Conclusions**

In this dissertation, the novel SOA-based photonic frequency-upconverter has been proposed. For the understanding of the characteristics of the proposed photonic upconverter, the numerical analysis has been made based on the linearized rate-equations of the SOA, and the experimental verification was qualitatively performed as well. The major features of the upconverter are as follows: First, the photonic frequency-upconversion can be achieved with SOA cross-gain modulation and PD square-law photo-detection. Second, the conversion efficiency is directly attributed by the SOA optical gain and can be optimized by either controlling the optical LO power or selecting the optical IF and LO wavelengths within the SOA optical gain bandwidth. Third, the IF frequency selection is determined by the SOA gain modulation bandwidth, whereas the LO frequency should be within the PD bandwidth. In addition, the conversion efficiency would not be much affected by the SOA input light polarizations as long as the polarization-insensitive SOA is used.

Using these useful features, the new radio-on-fiber architecture has been suggested where the base-band or IF-band WDM data are frequency-upconverted with a single optical LO source remotely at

base stations. In order to prevent the fiber dispersion-induced signal power suppression, the optical LO source under consideration should have two optical modes that are separated by the desired LO frequency and are well correlated for low phase-noise characteristics in photo-detection. The 60-GHz radio-on-fiber distribution of 2x622Mbps digital WDM channels was experimentally demonstrated.

## Appendix

### ◆ Fiber Dispersion Effect in intensity-modulation and direct-detection

The normalized electric field of the optical carrier is written [8]

$$E = \sqrt{P} e^{j(\omega_c t + \Phi(t; P))} \quad (\text{A.1})$$

where  $P$  is the optical power,  $\omega_c$  the angular optical carrier frequency and  $\Phi$  the optical phase of the electric field. For the Mach-Zehnder intensity modulator, the optical phase  $\Phi$  changes with the optical power  $P$  so that the chirp parameter  $\alpha$  can be defined as

$$\Delta\Phi = \frac{\alpha \Delta P}{2P} \quad (\text{A.2})$$

Eq. (A.2) for the frequency chirp parameter  $\alpha$  is also valid for a semiconductor laser if the adiabatic chirp is not taken into account. In this case,  $\alpha$  is given by [23]

$$\alpha = - \frac{\frac{\partial \eta}{\partial N}}{\frac{\partial g}{\partial N}} \quad (\text{A.3})$$

where  $\eta$  is the refractive index,  $N$  the carrier density and  $g$  is the modal gain.

In order to investigate the fiber dispersion effect, the small signal analysis is performed with Eq. (A.1) and (A.2). When the modulator is assumed to be intensity-modulated, its output can be written by:

$$P(t) = P_0 (1 + m_{IM} \cos(2\pi f_{LO} t)) \quad \text{with } m_{IM} \ll 1 \quad (\text{A.4})$$

where  $P_0$ ,  $m_{IM}$  and  $f_{LO}$  represents the average optical power, intensity-modulation index, and the electrical modulation angular frequency, respectively. Eq. (A.1) can be expressed with a Fourier series by using Eq. (A.2) and Eq. (A.4):

$$E(t) = \sum_{k=-\infty}^{\infty} A_k e^{j2\pi k f_{LO} t} \cdot e^{j\omega_c t} . \quad (\text{A.5})$$

For the case of the small  $m_{IM}$ , Eq. (A.1) can be simply re-written:

$$E(t) = (A_{-1}e^{-j2\pi f_{LO}t} + A_0 + A_{+1}e^{j2\pi f_{LO}t}) \cdot e^{j\omega_c t} \quad (\text{A.6})$$

where  $A_{\pm 1} = \sqrt{P_0} m_{IM} (1 + j\alpha)/4$  and  $A_0 = \sqrt{P_0}$ . Eq. (A.6) shows that the intensity-modulation of the optical light produces three spectral components: one optical center carrier at  $\omega_c$  and two sidebands separated by  $f_{LO}$  in the optical spectrum. These three components propagate through the single-mode fiber with the different velocities due to the fiber dispersion. The propagation constant is expressed by

$$\beta_k = \beta_0 \pm \frac{2\pi k f_{LO}}{v_g} - \frac{\pi \lambda_c^2 D k^2 f_{LO}^2}{c} \quad (\text{A.7})$$

where  $v_g$  is the group velocity,  $D$  the fiber chromatic dispersion parameter and  $\lambda_c$  the center optical carrier wavelength.

The output electric field after the dispersive fiber can be written:

$$E(t) = \sum_{k=0,\pm 1} A_k e^{j(2\pi k f_{LO} t - \beta_k L_f)} \cdot e^{j\omega_c t} \quad (\text{A.8})$$

where  $L_f$  is the fiber length. The fiber loss is not taken into account, here. The photo-detected current after the fiber can be obtained from

$I_{PD} = R_{PD}|E(t)|^2$  by using Eq. (A.8).  $R_{PD}$  is the PD responsivity. The photo-detected electrical power at  $f_{LO}$  is given by

$$P_{LO} \propto \cos^2\left(\frac{\pi\lambda_c^2 DL_f f_{LO}^2}{c} + \arctan(\alpha)\right). \quad (\text{A.9})$$

Eq. (A.9) shows clearly that the photo-detected LO power  $P_{LO}$  is periodically suppressed at

$$L_f = \frac{c}{2\lambda_c^2 D f_{LO}^2} \left(1 + 2k - \frac{2}{\pi} \arctan(\alpha)\right) \text{ with } k=0, 1, 2, \dots$$

as shown in Fig. 1.3 for  $f_{LO}=30$  GHz.

## References

- [1] A. J. Seeds, "Microwave Photonics," *IEEE Trans. Microwave Theory and Techniques*, vol. 50, no. 3, pp. 877-887, 2002.
- [2] T. Kosugi, T. Shibta, T. Enoki, M. Muraguchi, A. Hirata, T. Nagtsuma, and H. Kyuragi, "A 120-GHz millimeter-wave MMIC chipset for future broadband wireless access applications," in Tech. Dig. *Int'l Microwave Photonics '03*, pp. 129-132, 2003.
- [3] R. -P. Braun, G. Grosskopf, D. Rohde, F. Schmidt, and G. Walf, "Fiber-optic millimeter-wave generation at 64 GHz and spectral efficient data transmission for mobile communications," in Tech. Dig. *Optical Fiber Communications Conference (OFC'98)*, TuC4, pp. 17-18, 1998.
- [4] H. Harada, K. Sato, and M. Fujise, "A radio-on-fiber based millimeter-wave road-vehicle communication system by a code division multiplexing radio transmission scheme," *IEEE Trans. Intelligent Transportation Systems*, vol. 2, no. 4, pp. 165-179, 2001.
- [5] J. R. Cleveland, and L. S. Tamil, "Trunking of multiplexed RF channels to remote antennas with fiber optic links," in Tech. Dig. *Military Communications Conference (MILCOM '96)*, pp. 21-24, 1996.
- [6] J. M. Payne, and W. P. Shillue, "Photonic Techniques for local oscillator generation and distribution in millimeter-wave radio astronomy," *Tech. Dig. Int'l Microwave Photonics '02*, pp. 9-12, 2002.
- [7] S. Yamamoto, N. Edagawa, H. Taga, Y. Yoshida, and H. Wakabayashi, "Analysis of laser phase noise to intensity noise



conversion by chromatic dispersion in intensity modulation and direct detection optical-fiber transmission,” *J. Lightwave Technology*, vol. 8, no. 11, pp. 1716-1722, 1990.

- [8] F. Devaux, Y. Sirel, and J. F. Kerdiles, “Simple Measurement of Fiber Dispersion and of Chirp Parameter of Intensity Modulated Light Emitter,” *J. Lightwave Technology*, vol. 11, no. 12, pp. 1937-1940, 1993.
- [9] Y.-K. Seo, C.-S. Choi, W.-Y. Choi, "All Optical Signal Up-Conversion for Radio-on-fiber Applications Using Cross-Gain Modulation in Semiconductor Optical Amplifiers," *IEEE Photonics Technology Letters*, Vol.14, No.10, pp.1448-1450, 2002.
- [10] Y.-K. Seo, J.-H. Seo and W.-Y. Choi, "Photonic Frequency-Upconversion Efficiencies in Semiconductor Optical Amplifiers," *IEEE Photonics Technology Letters*, Vol.15. no.5, pp.751-753, 2003.
- [11] J.-H. Seo, Y.-K. Seo and W.-Y. Choi, "Spurious-Free Dynamic Range Characteristics of the Photonic Up-Converter Based on a Semiconductor Optical Amplifier," *IEEE Photonics Technology Letters*, Vol.15. no.11, pp.1591-1593, 2003
- [12] Y.-K. Seo, J.-H. Seo, and W.-Y. Choi, "60-GHz Radio-On-Fiber Distribution of 2 x 622 Mb/s WDM Channels Using Remote Photonic-Frequency Upconversion," *Microwave and Optical Technology Letter*, Vol. 39, No. 3, pp.201-203, 2003
- [13] M. Tsuchiya, and T. Hoshida, “Nonlinear Photodetection Scheme and Its System Applications to Fiber-Optic Millimeter-Wave Wireless Down-Links,” *IEEE Trans. on Microwave Theory and Techniques*, vol. 47, no. 7, pp. 1342-1350, 1999.
- [14] W. Shieh, S. X. Yao, G. Lutes, and L. Maleski, “An all-optical microwave mixer with gain,” in *Tech. Dig. OFC’97*, ThG1, pp.

263-264, 1997.

- [15] U. Gliese, "Coherent fiber-optic links for transmission and signal processing in microwave and millimeter-wave systems," in Tech. Dig. *Int'l Microwave Photonics '03*, pp. 211-214, 1998.
- [16] G. H. Smith, D. Novak, C. Lim, and K. Wu, "Technique for optical SSB generation to overcome dispersion penalties in fibre-radio systems," *Electron. Lett.*, vol. 33, no. 1, pp. 74-75, 1997.
- [17] J. Park, M. S. Shakouri, and K. Y. Lau, "Millimetre-wave Electro-optical upconverter for wireless digital communications," *Electron., Lett.*, vol. 31, no. 13, pp. 1085-1086, 1995.
- [18] L. N. Langley, M. O. Elkin, C. Edge, M. J. Wale, U. Gliese, X. Huang, and A. J. Seeds, "Packaged semiconductor laser optical phase-locked loop (OPLL) for photonic generation, processing and transmission of microwave signals," *IEEE Trans. Microwave Theory and Techniques*, vol. 47, no. 7, pp. 1257-1264, 1999.
- [19] L. Goldberg H. F. Taylor, and J. F. Weller, "FM sideband injection of diode lasers," *Electron. Lett.*, vol. 18, no. 23, pp. 1019-1020, 1982.
- [20] R. -P. Braun, G. Grosskopf, D. Rohde, and F. Schmidt, "Low-phase-noise millimeter-wave generation at 64 GHz and data transmission using optical sideband injection locking," *IEEE Photon. Technol. Lett.*, vol. 10, no. 5, pp. 728-730, 1998.
- [21] B. Cai, D. Wake, and A. J. Seeds, "Microwave frequency synthesis using injection locked laser comb line selection," in Dig. *LEOS summer topical meeting*, WD2, pp. 13-14, 1995
- [22] S. Kobayashi, Y. Yamamoto, M. Ito, and T. Kimura, "Direct frequency modulation in AlGaAs semiconductor lasers," *IEEE J. Quant. Electron.*, vol. QE-18, no. 4, pp. 582-595, 1982.

- [23] G. P. Agrawal, "Power spectrum of directly modulated single-mode semiconductor lasers: chirp-induced fine structure," *IEEE J. Quant. Electron.*, vol. QE-21, no. 6, pp. 680-686, 1985.
- [24] E. Peral and A. Yariv, "Large-signal theory of the effect of dispersive propagation on the intensity modulation response of semiconductor lasers," *J. Lightwave Technol.*, vol. 18, no. 1, pp. 84-89, 2000.
- [25] L. A. Johansson, and A. J. Seeds, "Millimeter-Wave Modulated Optical Signal Generation with High Spectral Purity and Wide-Locking Bandwidth Using a Fiber-Integrated Optical Injection Phase-Lock Loop", *IEEE Photon. Technol. Lett.*, vol. 12, no. 6, pp. 690-692, 2000.
- [26] A. C. Bordonalli, C. Walton, and A. J. Seeds, "High-Performance Phase Locking of Wide Linewidth Semiconductor Lasers by Combined Use of Optical Injection Locking and Optical Phase-Locked Loop", *J. Lightwave Technol.*, vol. 17, no. 2, pp. 328-342, 1999.
- [27] Y.-K. Seo, W.-Y. Choi, and A.-J. Kim, "Optical generation of 32 GHz millimeter-waves using side-mode injection-locking of semiconductor lasers," in *Dig. Conference on Optoelectronics and Optical Communications*, ThC2-5, pp. 239-240, 2000.
- [28] Y.-K. Seo, and W.-Y. Choi, "Influence of Unselected Master Laser Sidebands on the Spectral Characteristics of Beat Sideband Injection-Locking," in *Tech. Dig. Int'l Microwave Photonics'01*, pp. 109-112, 2001.
- [29] R. Lang, "Injection locking properties of a semiconductor laser," *IEEE J. Quant. Electron.*, vol. QE-18, no-6, pp. 976-983, 1982.
- [30] J. C. Cartledge and G. S. Burley, "The effect of laser chirping on lightwave system performance," *J. Lightwave Technol.*, vol. 7, no.

3, pp. 568-573, 1989.

- [31] J. Troger, P.-A. Nicati, L. Thevenaz, and Ph. A. Robert, "Novel measurement scheme for injection-locking experiments," *IEEE J. Quant. Electron.*, vol. 35, no. 1, pp. 32-38, 1999.
- [32] J. Troger, L. Thevenaz, P.-A. Nicati, and P.-A. Robert, "Theory and experiment of a single-mode diode laser subject to external light injection from several lasers," *J. Lightwave Technol.*, vol. 17, no. 4, pp. 629-636, 1999.
- [33] F. Mogensen, H. Olesen, and G. Jacobsen, "Locking conditions and stability properties for a semiconductor laser with external light injection," *IEEE J. Quant. Electron.*, vol. QE-21, no. 7, pp. 784-793, 1985.
- [34] D. Marcenac and A. Mecozzi, "Switches and Frequency Converters Based on Cross-Gain Modulation in Semiconductor Optical Amplifiers," *IEEE Photon. Technol. Lett.*, vol. 9, no. 6, pp. 749-751, 1997.
- [35] H. Lee, H. Yoon, Y. Kim and J. Jeong, "Theoretical Study of Frequency Chirping and Extinction Ratio of Wavelength-Converted Optical Signals by XGM and XPM Using SOA's," *IEEE Quantum Electron.*, vol. 35, no. 8, pp. 1213-1219, 1999.
- [36] J. S. Lee, J. R. Kim, S. Park, M. W. Park, J. S. Yoo, S. D. Lee, A. G. Choo and T. I. Kim, "Spot Size Converter Integrated Semiconductor Optical Amplifier," in *Tech. Dig. CLEO/Pacific Rim '99*, pp. 1155-1156, 1999.

## 국문 요약

### WDM / 광대역 Radio-on-Fiber 응용분야를 위한

### 반도체 광증폭기를 이용한

### 포토닉스 주파수 상향 기법 연구

반도체 광증폭기 (SOA)의 상호이득변조와 광검출기 (PD)의 자승 광검출 특성을 이용하여, 광학적 LO 신호원을 통해 광학적 기저대역이나 IF 주파수 대역 신호의 주파수 상향이 가능토록 하는 새로운 포토닉스 주파수 상향 기법을 제안하고 있다. 광섬유 영향을 배제하기 위해 광학적 헤테로다인 방식의 sideband injection locking 기법을 이용하여, 광스펙트럼에서 원하는 LO 주파수 차이만큼 떨어진 두 개의 광학 모드를 갖는 광학적 LO 신호원을 생성하였다. 두 광학 모드들간의 beat signal로서 검출된 LO 신호원은 좁은 선폭과 장시간 출력세기의 안정성을 갖는다.

선형 SOA 비울방정식을 바탕으로 제안된 포토닉스 주파수 상향기의 수치적인 해석을 통해, 상향 효율은 SOA 광이득과 직접적으로 관련이 있으며, 광 LO 신호의 크기를 조절하거나 IF와 LO 파장을 조절함으로써 최적화가 가능함을 알 수 있었다. 실험적인 검증도 정성적으로 함께 수행되었다.

이러한 유용한 특성을 이용하여, base station까지의 20-km 유선 광통신 링크, base station에서의 광 LO 신호원을 이용한 광대역 WDM 데이터의 원격 주파수 상향, 그리고 3-meter 무선 링크로 구성된 60-GHz radio-on-fiber 분배 구조에서 622 Mbps 광대역 디지털 WDM 두 채널의 전송 데모를 실험적 수행하였다. 파장으로 구별되는 복수 base station들이 하나의 광학적 LO 신호원을 공유하는 radio-on-fiber 시스템에서, 제안되고 있는 구조는 매우 유용할 것이다.

---

핵심되는 단어: radio-on-fiber, 반도체 광증폭기, 상호이득변조, sideband injection locking, 광학적 헤테로다인 기법, 원격 포토닉스 주파수 상향 기법, 변환 효율, 파장분할다중화기법